Computation of Thomson spectra for anisotropic relativistic electron-velocity distributions

van Est, Q.C.

Award date:
1989

H443+H444(ON)
→ NL.4
4×

COMPUTATION OF THOMSON SPECTRA FOR ANISOTROPIC RELATIVISTIC ELECTRON-VELOCITY DISTRIBUTIONS

Q.C. van Est

I.R. 89/003

FOM-Instituut voor
Plasmafysica
Rijnhuizen
Nieuwegein

I.R. 89/003
april 1989

COMPUTATION OF THOMSON SPECTRA FOR ANISOTROPIC RELATIVISTIC ELECTRON-VELOCITY DISTRIBUTIONS

by Q.C. van Est

With thanks to my parents, André van Lammeren, Rolie Barth, Geert Verhaag, Tony Donné, Luuk Ornstein and fellow-students.

This work was performed as part of the research programme of the association agreement of Euratom and the "stichting voor Fundamenteel Onderzoek der Materie" (FOM) with financial support from the "Nederlandse Organisatie voor Zuiver-Wetenschappelijk Onderzoek" (ZWO) and Euratom.

Table of Contents

Abstract 1

Table of contents 2

Chapter I. Introduction 3

I.1 The TORTUR tokamak
I.2 The discharge
I.3 Diagnostics
I.4 Thomson scattering device
I.5 The scattered spectrum
I.6 Observation on non-Maxwellian electron distributions
I.7 Research aim

Chapter II. Scattered spectra for an isotropic electron velocity distribution function 8

II.1 Relativistic scattering from a single electron
II.2 Relativistic scattering from a plasma
II.3 Scattered spectrum for a relativistic Maxwellian

Chapter III. Scattered spectra for an anisotropic electron velocity distribution function . 17

III.1 Scattered spectra for a shifted relativistic Maxwellian
III.1.1 Small drift velocities : $\beta_d \leq 0.005$
III.1.2 Large drift velocities : $0.1 \leq \beta_d \leq 0.4$
III.1.2.1 Doppler shift
III.1.2.2 Scattered intensities
III.2 Scattered spectra for a bi-Maxwellian
III.1 Scattered spectra for a relativistic bobtail distribution

Chapter IV. Geometrical considerations on Thomson scattering . . 28

IV.A1 Transformation matrix from $(\beta_x, \beta_y, \beta_z)$ to $(\beta_k, \beta_{k\perp}, \beta_{kT})$
IV.A1 Transformation of the area dA

Summary 33

References 34

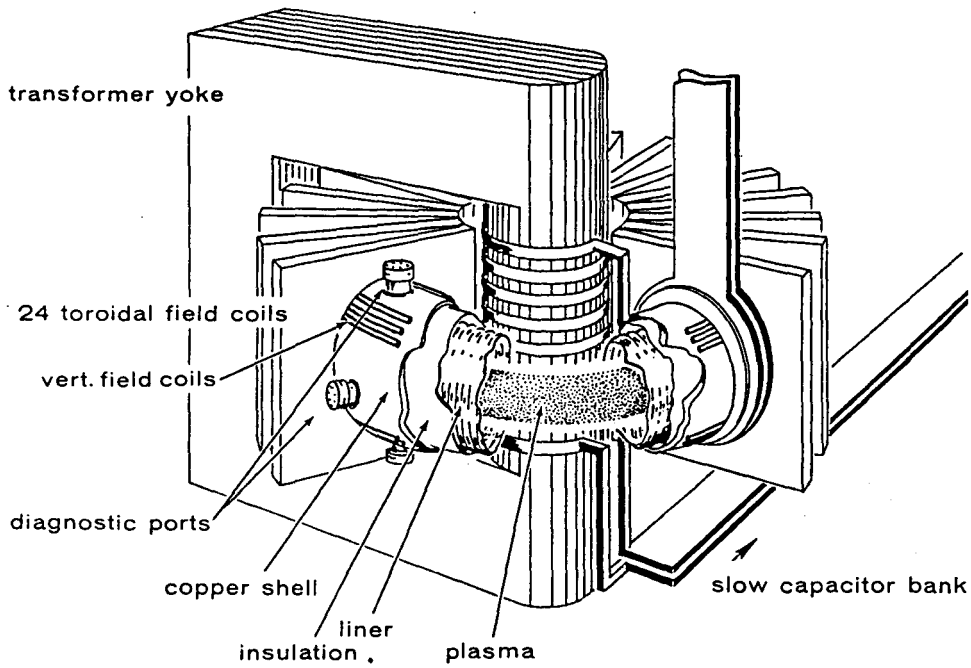

Fig.1.1 Schematic view of the TORTUR tokamak.

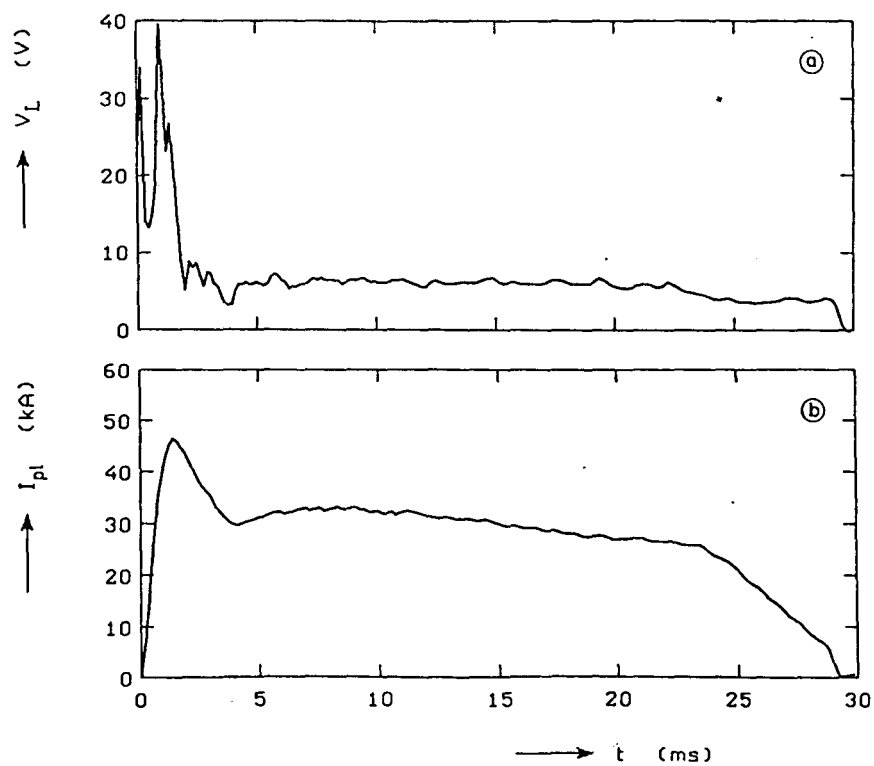

Fig.1.2 Typical signals of the plasma current (I_p) and the loop voltage (V_L).

I.Introduction

The aim of the fusion research programme is to find out wether it is possible to create, in a controlled and potentially useful way, high temperature matter in which thermonuclear fusion reactions between light nuclei can produce a net yield of energy. Because fusion reactions occur between charged nuclei and because the fusion cross sections are much smaller than the Coulomb cross section for scattering, it follows that to achieve a net energy gain a hot gas with a temperature of $\sim 10keV$ ($\sim 10^8 K$) is required. A gas at this temperature is fully ionized and as such constitutes, in the case of hydrogen, a plasma with closely equal number densities of electrons and ions.

Such a hot gas must clearly be kept away from material walls. This can be done by magnetic confinement. The tokamak is the most advanced of several classes of toroidal magnetic confinement systems. It was pioneered in the Soviet Union in the 1960's. There are now many of these machines around the world with very different sizes and research aims. The Joint European Torus (JET) device is the largest magnetic confinement machine in the world both in physical size and in magnitude of the plasma current ($I_p \sim 7MA$).

I.1 The TORTUR tokamak

The TORTUR tokamak at the FOM Institute for Plasma Physics at Nieuwegein was a small tokamak ($I_p \leq 55kA$). It was originally build in the mid 70's to study the physics of a mildly turbulent plasma. In a tokamak the required confining magnetic field is produced by the combination of a toroidal current in the plasma itself and currents in external poloidal coils. The current is driven through the plasma by operating the plasma ring as the secondary coil of a transformer. The current will both heat up the plasma ($\sim 1keV$ at TORTUR) by ohmic dissipation and generate a poloidal magnetic field. This poloidal magnetic field will add up to the steady toroidal field, generated by the external coils, to yield a helical field configuration. Together with an additional vertical field and a horizontal field for plasma positioning, this field configuration ensures stable confinement under well-defined conditions.

Table 1.1 Machine parameters.

tokamak type	JET	TORTUR
major radius R (m)	3.0	0.46
minor radius a (m)	1.2	0.085
toroidal magnetic field B_T (T)	3.4	2.9

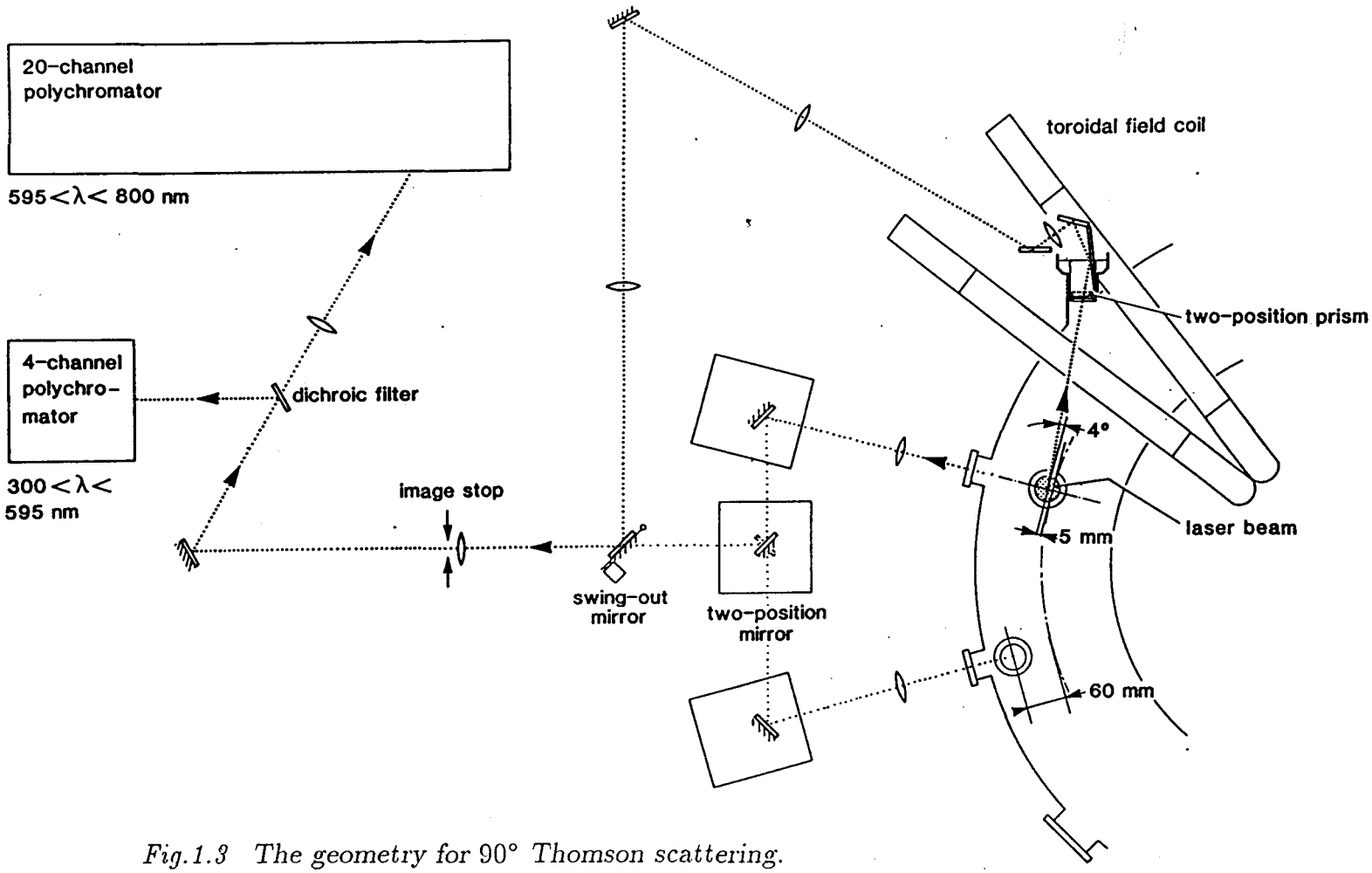

Fig.1.3 The geometry for 90° Thomson scattering.
The laser beam is directed vertically through the plasma. The scattered light can be collected in two different directions : parallel and perpendicular to the magnetic axis, and is led in either case to the polychromators for recording. Radial scattering can be performed at two different positions $r = 5mm$ and $r = 60mm$.[Barth, 1987]

I.2 The discharge

The formation of a plasma is initiated by pre-ionization of the hydrogen gas. The discharge is then started by a fast capacitor bank which rapidly forms a hot plasma. This plasma formation stage is characterized by a steep rise of the plasma current. After a few milli-seconds an electrolytic bank takes over the magnetization and maintains a steady plasma current (plateau phase) until saturation of the transformer yoke puts an end to the discharge. *Fig.1.2* shows a typical signal of the plasma current during a TORTUR discharge.

I.3 Diagnostics

Clearly it is important to have accurate and reliable measurements of the plasma conditions. Except at the extreme edge of the plasma, material probes cannot be used. Therefore we use either passive methods to measure the magnetic fields or to analyse radiation and particle emission from the plasma or active methods where radiation or particles from an external source are used to probe the plasma. For the TORTUR IV experiment (June 1987 - October 1988) the operational diagnostics were :

- Rogowski coils (determination of the plasma curent)
- Voltage loop (determination of the loop voltage)
- Sinus-cosinus coil set (recording of the plasma position)
- Electrostatic analyser (mass and energy determination of neutral particles)
- Electron cyclotron emission (ECE) polychromator (measurements of the time-resolved electron temperature profiles and deviations due to non-thermal populations)
- Time-of-flight analyser (determination of the velocity distribution of low energy neutrals from the edge of the plasma)
- Four channel soft X-ray detector (recording of the X-ray flux, to monitor the electron temperature and to determine the effective ion charge, Z_{eff})
- Collective scattering device (analysis of density fluctuations)
- Thomson scattering device (determination of the local electron temperature, density and current density)

I.4 Thomson scattering device

Although several diagnostic methods can be used to measure the electron temperature and density, the most direct and unambiguous method is Thomson scattering. The Thomson scattered spectrum reflects the velocity distribution function of the electrons in the scattering volume. Furthermore, the intensity of the scattered radiation integrated over all wavelengths is proportional to the number of electrons in the scattering volume. Thomson scattering thus provides the opportunity of measuring both the electron density and the electron temperature at selected points in the plasma.

In the TORTUR experiment we used a single-point 90° Thomson-scattering arrangement. This technique is illustrated in *Fig.1.3* and *Fig.1.4*. The light of a $300MW$ ruby laser ($\lambda_o = 694.3nm$), with a $20ns$ pulse duration, is focussed to a narrow beam and

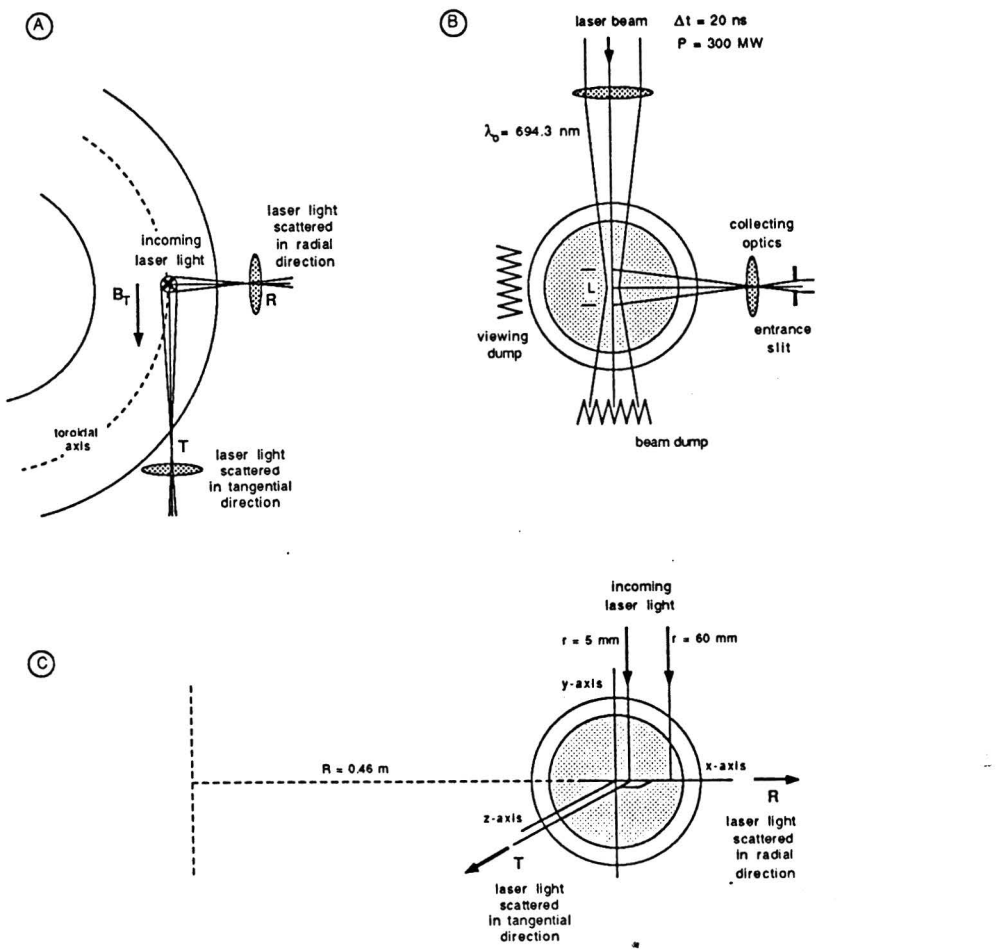

Fig.1.4 *Definition of the tangential and radial direction.*
A) top view of the torus, the toroidal magnetic field B_T is directed along the toroidal axis;
B) scattering geometry (poloidal cross section of the torus);
C) definition of the (x, y, z) coordinate system referring to the torus.
TORTUR values are : major radius $R = 0.46m$, minor radius $a = 0.085m$ and $B_T \leq 2.9T$.

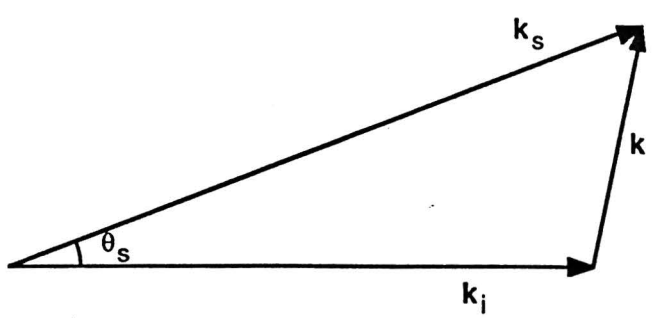

Fig.1.5 *The scattering process. The incoming wave vector $\mathbf{k}_i$, the scattered wave vector $\mathbf{k}_s$ and the scattering vector $\mathbf{k}$ are related by $\mathbf{k} = \mathbf{k}_s - \mathbf{k}_i$.*

directed vertically through the plasma at the radial positions $r = 5$ or $60mm$. Photons within a volume with a certain length L which are scattered from free electrons through the angle $\theta_s = 90°$ within a solid angle $d\Omega$ can be observed by a detector. At $r = 5mm$ the scattered spectrum can be observed both in radial and tangential directions [Barth, 1987]. [1]

The scattering volume is defined by the length L of the focussed laser beam and the diameter of the laser beam, which is about $1.3mm$ for TORTUR.

Table 1.2 Scattering parameters.

scattering direction	radial	tangential
radial position r (mm)	5 and 60	5
length of the scattering volume L (mm)	10	23
solid angle $d\Omega$ (sr)	$2 \cdot 10^{-2}$	$4 \cdot 10^{-3}$

I.5 The scattered spectrum

The Thomson spectrum, for laser light scattered by a plasma, is broadened with respect to that of the incoming beam by the Doppler shifts arising from the randomly moving electrons. The frequency of the waves scattered by an electron with velocity, $\mathbf{v}$, will suffer a Doppler shift, $\Delta\omega$:

$$\Delta\omega = \mathbf{k} \cdot \mathbf{v}, \tag{1.1}$$

where $\mathbf{k} = \mathbf{k}_s - \mathbf{k}_i$, and $\mathbf{k}_i$ ($\mathbf{k}_s$) is the wavevector of the incident (scattered) wave (*Fig.1.5*). The Thomson-scattered spectrum will represent the projection of the velocity distribution function on the scattering vector $\mathbf{k}$. For radial measurements $\mathbf{k}_i$ and $\mathbf{k}_s$ are both in the poloidal plane. So, radial measurements result in an observation of the electron-velocity distribution perpendicular to the toroidal magnetic field. Tangential scattering, with $\mathbf{k}_s$ along the toroidal axis, has its k-vector under 45° with the toroidal magnetic axis.

When a plasma is in equilibrium the electron velocities are distributed according to a Maxwellian distribution function. As noted the light scattered by the electrons will be Doppler broadened. When a equilibrium plasma is illuminated by a laser beam the scattered spectrum will have an almost Gaussian shape. The electron temperature can then be deduced from the width of the spectrum.

[1] Radial (R) and tangential (T) means perpendicular and parallel to the toroidal axis, respectively.

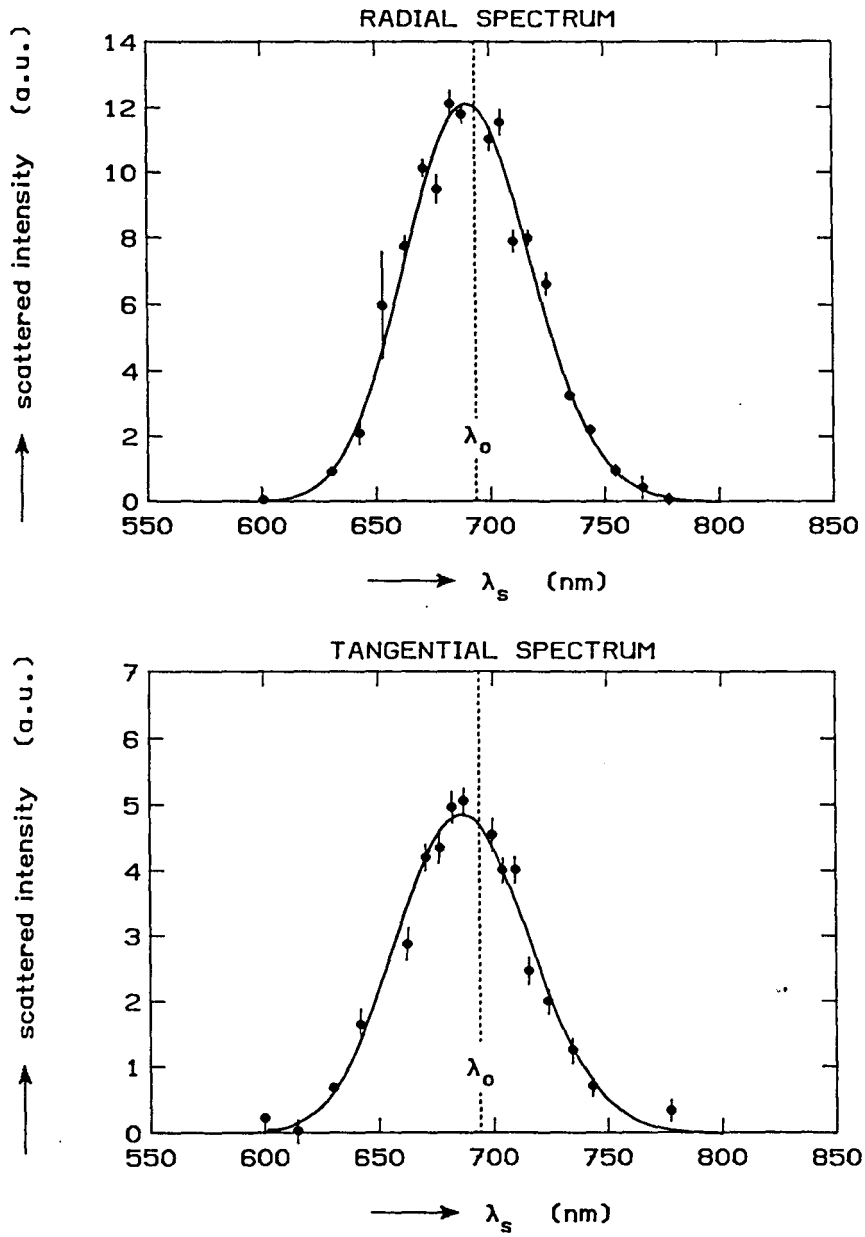

Fig.1.6 Measured Thomson spectra at TORTUR ($T_e \approx 400eV$, $n_e \approx 6 \cdot 10^{19} m^{-3}$).

I.6 Observation of non-Maxwellian electron distributions

Recording of the scattered spectrum is performed by a twenty-channel polychromator [Barth, 1984], equipped with infrared sensitive photomultipliers. The polychromator has an overall transmission of $\sim 45\%$ and covers a spectral range from 600 to $800nm$, which allows the detection of electron temperatures from $5eV$ to $2keV$. This large dynamic range is realized by using a different spectral bandwidth for the various channels (close to the laserline 4.5 and $13nm$ at the edge of the spectrum).

Owing to the high sensitivity and high resolution of the polychromator electron temperatures up to $1keV$ at a density of $5 \cdot 10^{19} m^{-3}$ can be measured with a statistical error of $\approx 1\%$. These properties also enable the detection of irregularities in the velocity distribution. At the TORTUR tokamak distortions in the electron-velocity distribution were observed (see *Fig. 1.6*). In many observed spectra distortions are found on the almost Gaussian profile at $\Delta\lambda \approx 23nm$, corresponding to $v \approx 7 \cdot 10^6 m/s$ The partial densities of the electron populations responsible for the distortions are found to be in the order of 1-5%. One of the possible explanations for the occurence of these dips is thought to be the existence of magneto-sonic waves, such as Alfvén waves, since the distortions are strongest at a wavelenght shift which corresponds to the Alfvén velocity [De Kluiver *et al.*, 1988]. [1] Comparable distortions are found in plasmas of other devices but are ascribed to suprathermal electrons [Bartiromo *et al.*, 1979], runaway electrons [Pieroni *et al.*, 1975; Tartari, 1984], or trapped particles [Blokh *et al.*, 1981].

I.7 Research aim

To simulate the non-thermal features observed in the radial TORTUR spectra a computer-code is written for calculating the Thomson spectrum for an anisotropic electron-velocity distribution function. The code is based on the theory of relativistic Thomson scattering.

The decision to write such a computer-code was made in spring '88. At that time the tangential measurements were about to be implemented. These observations were expected to give further indication about the origin of the distortions. However, interpreting and relating the radial and tangential spectra was found to compel a thorough insight of the Thomson-scattering theory. Writing a computer-code based on the Thomson-scattering theory imposes equal demands. Furthermore, it will help to comprehend the implications made by the theory. Our aim is thus to get a better insight in the relation between the electron-velocity distribution and the related Thomson-scattered spectrum.

This report follows the course of the research programme. In chapter II an introduction to the incoherent relativistic scattering theory is given. Initially a code is written for calculating the spectrum for an isotropic velocity distribution. For a relativistic Maxwellian distribution an analytic expression is obtained for the scattered spectrum wich serves as a check-up for the "isotropic code". Chapter III provides an integral-expression for

[1] Alfvén velocity $v_a = B(\mu_0 n_i m_i)^{-1/2} \approx 6 \cdot 10^6 m/s$ (B, n_i, m_i are : the magnetic field strength, the ion density and the ion mass, respectively).

calculating the spectrum for an anisotropic distribution on basis of which a computer-code is written. A first check on the "anisotropic code" is provided by the calculated spectra from the former chapter. Furthermore, high velocity effects are studied by use of the "anisotropic code". Finally, in chapter IV, Thomson scattering is treated from a geometrical point of view.

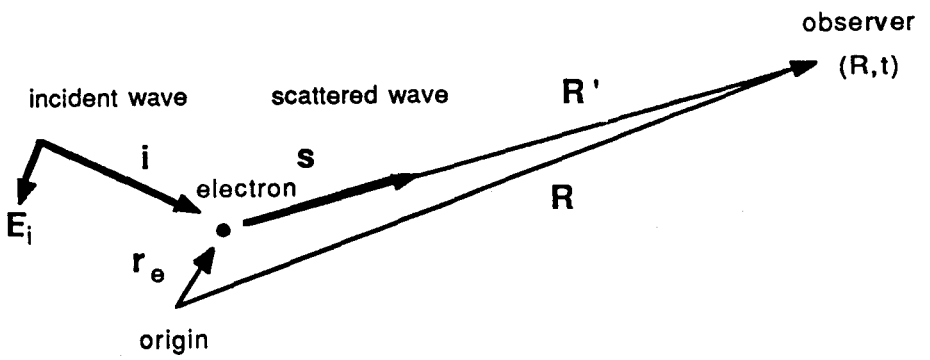

Fig.2.1 Diagram illustrating the scattering proces.

II.Scattered spectra for an isotropic electron-velocity distribution function

This paragraph is meant as a first introduction to the Thomson-scatttering theory and is based on an article by M. Mattioli "Incoherent light scattering from high temperature plasmas" (1974). In this article an analytic expression is obtained for the scattered spectrum for a relativistic Maxwellian distribution. It also provides an integral-expression for calculating the spectrum for an isotropic velocity distribution.

It should be stressed that this section is not intended to give a complete description of the Thomson-scattering theory. Its purpose is merely to point out both the physical mechanism involved and the assumptions made in deriving an expression for the scattered spectrum [Evans and Katzenstein, 1969; Nielsen, 1982; Sheffield, 1972].

II.1 Relativistic scattering from a single electron

Because we use an optical laser we may, in the derivation of the scattering cross-section, neglect the Compton effect, since in this case the energy of the photon is much smaller than the electrons' rest energy. Therefore a classical treatment will suffice.

In this case we should keep in mind the following physical picture. An electromagnetic wave is incident on a charged particle, the charge is accelerated by the oscillating fields of the radiation and as an effect it radiates its own electromagnetic waves at the time t'; we will call this the retarded time. Finally, this radiation is observed at the time t.

Let us consider a single electron at the position $\mathbf{r}_e(t')$, with the normalized velocity $\boldsymbol{\beta} = \mathbf{v}_e/c$, and an incident monochromatic plane wave of frequency ω_i (i=incident) and wave vector $\mathbf{k}_i = k_i\mathbf{i}$ (see *Fig 2.1*). In this case $\mathbf{i}$ is the unit vector in the direction of the incident radiation. The electric field in the laboratory frame, at the position of the electron, can be described as :

$$\mathbf{E}_i(\mathbf{r}_e, t') = \mathbf{E}_{i0}\cos(\mathbf{k}_i \cdot \mathbf{r}_e - \omega_i t'). \tag{2.1}$$

The magnetic field $\mathbf{B}_i$ is :

$$\mathbf{B}_i(\mathbf{r}_e, t') = \mathbf{i} \times \mathbf{E}_i(\mathbf{r}_e, t')/c. \tag{2.2}$$

Acceleration of the electron by this e. m. wave is described by the equation of motion :

$$\frac{d}{dt} m_0 \gamma \boldsymbol{\beta} = -e\Big[\mathbf{E}_i/c + \boldsymbol{\beta} \times \mathbf{B}_i\Big], \tag{2.3}$$

where $\gamma = [1-\beta^2]^{-1/2}$, m_0 is the electron rest mass and e is the elementary charge.

After substitution of (2.2), the next equation can be derived for the acceleration $\dot{\boldsymbol{\beta}}$:

$$c\dot{\boldsymbol{\beta}}(\mathbf{r}, t') = -\frac{e}{m_0\gamma}\Big[\mathbf{E}_i + \boldsymbol{\beta} \times (\mathbf{i} \times \mathbf{E}_i) - \boldsymbol{\beta}(\boldsymbol{\beta} \cdot \mathbf{E}_i)\Big]. \tag{2.4}$$

As mentioned before, the accelerated electron will radiate an electromagnetic wave, called the scattered wave.

The electric field $\mathbf{E}_s$ (s=scattered), at the fixed position $\mathbf{R}'$ and at the time t, scattered by an electron accelerated by an electromagnetic wave at the position $\mathbf{r}_e$ and at the time t', is given by the following formula obtained from the Liénard-Wiechart potentials : [1]

$$\mathbf{E}_s(\mathbf{R}',t) = \frac{e}{4\pi\varepsilon_0}\left[\frac{(\mathbf{s}-\boldsymbol{\beta})}{\gamma^2(1-\mathbf{s}\cdot\boldsymbol{\beta})^3 R'^2}\right]_{ret} + \frac{e}{4\pi\varepsilon_0 c}\left[\frac{\mathbf{s}\times[(\mathbf{s}-\boldsymbol{\beta})\times\dot{\boldsymbol{\beta}}]}{(1-\mathbf{s}\cdot\boldsymbol{\beta})^3 R'}\right]_{ret}, \tag{2.5}$$

where $\mathbf{s} = \mathbf{R}'/R'$ is the unit vector in the direction of observation. This electric field is naturally divided in a "velocity field", which is independent of acceleration, and an "acceleration field", depending linearly on $\dot{\boldsymbol{\beta}}$. The velocity field is a static field which falls off as R^{-2} and can be neglected with respect to the acceleration field in the far-field region. The acceleration field is a typical electromagnetic radiation field : both $\mathbf{E}$ and $\mathbf{B}$ being transverse to the line of sight and varying as R^{-1}.

The next step is to find the relation between the retarded time and the time at which the scattered wave is being observed. For achieving this, we use a straight-line approximation. For this we must assume that the plasma electrons are unperturbed by the electromagnetic field and we neglect the curvature of their trajectories caused by the static magnetic field. We therefore, introduce for $\mathbf{r}_e(t)$ the unperturbed orbit :

$$\mathbf{r}_e(t) = \mathbf{r}_e(0) + \boldsymbol{\beta} ct. \tag{2.6}$$

If we put this into the argument of the cosine of eq.(2.1), this becomes :

$$\mathbf{k}_i \cdot \mathbf{r}_e(t') - \omega_i t' = \mathbf{k}_i \cdot \mathbf{r}_e(0) - [1 - \mathbf{i}\cdot\boldsymbol{\beta}]\omega_i t'. \tag{2.7}$$

This result states that the electron sees a reduced frequency due to its own motion.

The field observed at a distance R' and at the time t is related to the behaviour of the charge at a previous time t', the retarded time. From the geometry it follows :

$$t' = t - R'/c. \tag{2.8}$$

Since we are interested in scattering volumes whose dimensions are small compared to the distance of observation ($r_e \ll R$), we may write R' as :

$$\begin{aligned} R' &= |\mathbf{R} - \mathbf{r}(t')| \\ &\approx [R - \mathbf{s}\cdot\mathbf{r}_e(t')]. \end{aligned} \tag{2.9}$$

Inserting this in equation (2.8), and using equation (2.6), gives the following relation between the observers' time t and the retarded time t' :

$$t'[1 - \mathbf{s}\cdot\boldsymbol{\beta}] = t - [R - \mathbf{s}\cdot\mathbf{r}_e(0)]/c \tag{2.10}$$

[1] formula 14.14 in "Classical Electrodynamics" by J. D. Jackson.

Using expression (2.10) and putting this in equation (2.7), the phase of the electromagnetic field at the retarded time t' becomes :

$$\begin{aligned}\mathbf{k}_i \cdot \mathbf{r}_e(0) - [1 - \mathbf{i} \cdot \boldsymbol{\beta}]\omega_i t' &= -\omega_i(t - [R - \mathbf{s} \cdot \mathbf{r}_e(0)]/c)\frac{(1 - \mathbf{i} \cdot \boldsymbol{\beta})}{(1 - \mathbf{s} \cdot \boldsymbol{\beta})} + \mathbf{k}_i \cdot \mathbf{r}_e(0) \\ &= -\omega_s^*(t - [R - \mathbf{s} \cdot \mathbf{r}_e(0)]/c) + \mathbf{k}_i \cdot \mathbf{r}_e(0) \\ &= \frac{\omega_s^*}{c}R - \omega_s^* t + \left(\mathbf{k}_i - \frac{\omega_s^* \mathbf{s}}{c}\right) \cdot \mathbf{r}_e(0) \\ &= \mathbf{k}_s \cdot \mathbf{R} - \omega_s^* t - \mathbf{k} \cdot \mathbf{r}_e(0), \end{aligned} \tag{2.11}$$

where

$$\omega_s^* = \omega_i \frac{(1 - \mathbf{i} \cdot \boldsymbol{\beta})}{(1 - \mathbf{s} \cdot \boldsymbol{\beta})}, \tag{2.12}$$

and

$$\mathbf{k} = \mathbf{k}_s - \mathbf{k}_i = \frac{\omega_s^*}{c}\mathbf{s} - \frac{\omega_i}{c}\mathbf{i}. \tag{2.13}$$

The frequency ω^* is the observed Doppler shifted frequency, caused by the motion of the electron relative to the incident photon and relative to the observer.

With equation (2.11) we can evaluate the acceleration field term in expression (2.5) at the retarded time. We get :

$$\begin{aligned}\mathbf{E}_s(\mathbf{R}', t) = \frac{r_0}{\gamma R}\left[\frac{\mathbf{s} \times \{(\mathbf{s} - \boldsymbol{\beta}) \times (\mathbf{E}_{i0} + \boldsymbol{\beta} \times (\mathbf{i} \times \mathbf{E}_{i0}) - \boldsymbol{\beta}(\boldsymbol{\beta} \cdot \mathbf{E}_{i0}))\}}{(1 - \mathbf{s} \cdot \boldsymbol{\beta})^3}\right] \\ \times \cos\left(\mathbf{k}_s \cdot \mathbf{R} - \omega_s^* t - \mathbf{k} \cdot \mathbf{r}_e(0)\right), \end{aligned} \tag{2.14}$$

where $r_0 = e^2/4\pi\varepsilon_0 m_0 c^2 = 2.82 \cdot 10^{-15} m$ is the classical electron radius.

With obtaining the above formula, we are in the possession of all the fundamentals for deriving the scattering cross-section σ_s. The scattering cross-section is defined as the power (P_s) scattered per solid angle ($d\Omega$) divided by the incident power. The latter is given by the Poynting vector $\mathbf{S}_i$, which is proportional to the square of the incoming electric field strength.

To find the scattering cross-section as function of frequency $\sigma_s(\omega_s)$ (formally : the scattering cross-section per unit frequency interval), we should derive the scattered light intensity as function of frequency. In mathematical terms :

$$\sigma_s(\omega_s) = P_s(\omega_s)/S_i d\Omega, \tag{2.15}$$

where $S_i = c\varepsilon_0 |\mathbf{E}_{i0}|^2$.

More specifically, the power radiated by the electron at the frequency ω_s is proportional to the square of the Fourier component of frequency ω_s, which is defined by :

$$\mathbf{E}_s(\mathbf{R}', \omega_s) = \frac{1}{T}\int_{-T/2}^{T/2} \mathbf{E}_s(\mathbf{R}', t) e^{i\omega_s t}\, dt \tag{2.16}$$

So we may write the power scattered by a single electron per unit frequency interval $P_s(\omega_s)$, received during a large time interval $-T/2 \leq t \leq T/2$, by a detector placed at R, which subtends the solid angle $d\Omega$, as :

$$P_s(\omega_s) = \lim_{T\to\infty} \frac{cR^2 d\Omega}{4\pi^2 T} \left| \int_{-T/2}^{T/2} \mathbf{E}_s(\mathbf{R}', t) e^{i\omega_s t}\, dt \right|^2 . \tag{2.17}$$

In doing this, we have linked the radiating power as a function of frequency to the time-dependent scattered electric field. So, by combining equation (2.14), (2.15) and (2.17) we have in principle solved our problem.

Before getting trapped in the labyrinth of formulas, let us consider the geometrical set-up, described in section I.4, to simplify the scattered field equation (2.14).

In most cases a plane polarized wave, with the incident electric field $\mathbf{E}_i$ perpendicular to the scattering plane is chosen. [1] In addition we will use a polarizer to select the scattered light polarized parallel to the incident electric field. If $\mathbf{i}$, $\mathbf{s}$ and $\mathbf{e}_i$ are the unit vectors parallel, to the incident wave vector $\mathbf{k}_i$, to the scattered wave vector $\mathbf{k}_s$, and to the electric field, respectively, we define :

$$\beta_i = \mathbf{i} \cdot \boldsymbol{\beta}, \quad \beta_s = \mathbf{s} \cdot \boldsymbol{\beta} \quad \text{and} \quad \beta_E = \mathbf{e}_i \cdot \boldsymbol{\beta}. \tag{2.18}$$

Remembering, that $\omega_s^* = \omega_i(1-\beta_i)/(1-\beta_s)$, we can derive, for the chosen experimental set-up, for a scattering angle θ_s : [2] , [3]

$$\mathbf{E}_s(R') = \frac{r_0}{\gamma R'} \frac{\omega_s^*}{\omega_i} \frac{1}{(1-\beta_s)} \left[1 - \beta_E^2 \frac{(1-\cos\theta_s)}{(1-\beta_i)(1-\beta_s)} \right], \tag{2.19}$$

where we have left out the time-varying part.

Inserting equation (2.19) in (2.17) and connecting this formula to expression (2.15), we get, after several non-trivial steps [Salzmann, 1986; Kukushkin, 1981], the scattering cross-section per unit frequency for scattering of light from a single electron moving with the speed $\boldsymbol{\beta}$:

$$\sigma_s(\omega_s, \theta_s) = \frac{r_0^2}{\gamma^2} \frac{\omega_s^{*2}}{\omega_i^2} \frac{1}{(1-\beta_s)} \left[1 - \beta_E^2 \frac{(1-\cos\theta_s)}{(1-\beta_i)(1-\beta_s)} \right]^2 \delta(\omega_s - \omega_s^*). \tag{2.20}$$

Here the delta function selects only those electrons having the right velocity for contributing to the scattering cross-section at the frequency ω_s. The factor γ^{-2} gives the decrease in scattering because of the relativistic increase in mass and corresponding decrease in effective "radius" of the electron.

Finally, we will write the scattering cross-section as function of scattered wavelength λ_s. With $\omega_s = 2\pi c/\lambda_s$, it follows :

$$d\omega_s = -\frac{2\pi c}{\lambda_s^2}\, d\lambda_s = -\omega^2 \frac{d\lambda_s}{\lambda_i} \omega_i, \tag{2.21}$$

---

[1] This means : $\mathbf{i} \cdot \mathbf{E}_i = \mathbf{s} \cdot \mathbf{E}_i = 0$.

[2] $\cos\theta_s = \mathbf{s} \cdot \mathbf{i}$.

[3] use the vector relation : $\mathbf{x}_1 \times \mathbf{x}_2 \times \mathbf{x}_3 = \mathbf{x}_2(\mathbf{x}_1 \cdot \mathbf{x}_3) - \mathbf{x}_3(\mathbf{x}_1 \cdot \mathbf{x}_2)$.

where ω is defined by :

$$\omega = \frac{\omega_s}{\omega_i} = \frac{\lambda_i}{\lambda_s}. \tag{2.22}$$

Using :

$$\sigma_s(\lambda_s, \theta_s) = \sigma_s(\omega_s, \theta_s)\frac{d\omega_s}{d\lambda_s}, \tag{2.23}$$

and the definition of ω, equation (2.20) becomes :

$$\sigma_s(\lambda_s, \theta_s) =$$

$$r_0^2 \frac{\omega^2}{\lambda_i} \frac{(1-\beta^2)}{(1-\beta_s)^5} \left[(1-\beta_i)(1-\beta_s) - \beta_E^2(1-\cos\theta_s)\right]^2 \delta\left(\omega - \frac{(1-\beta_i)}{(1-\beta_s)}\right). \tag{2.24}$$

II.2 Relativistic scattering from a plasma

Derivation of the cross section in the previous chapter showed that the cross section for scattering of light from a charged particle is inversely proportional to the square of its mass (see formula (2.24), where $r_0^2 \propto m_0^{-2}$). Therefore, when we consider scattering from a plasma, we can state that practically only the electrons contribute and that the contribution of the ions can be neglected.

Next, as in all scattering from an ensemble of particles, we should, in calculating the total scattered power, investigate whether the phase relations between the various scatterers must be taken into account. The quantity we use to determine this, is known as the scattering parameter α :

$$\alpha = \frac{\lambda_o}{4\pi\lambda_D \sin\theta_s/2}, \tag{2.25}$$

where λ_o is the central wavelength, θ_s is the scattering angle and λ_D is the Debye length :

$$\lambda_D = \left[\frac{\varepsilon_0 k T_e}{n_e e^2}\right]^{1/2}. \tag{2.26}$$

The Debye length is a measure of the shielding distance for an electric field in a plasma. Whenever local concentration of charge arises or external potentials are introduced into the plasma, these are shielded off over a distance comparable to the Debye length. This means that fluctuations on a length scale much smaller than the Debye length are occuring independently from each other. So, using a source that emits an electromagnetic wave with a wavelength, which is sufficiently small as compared to the Debye length, the phases of the wavelets $\mathbf{E}_s^i$, radiated by the different accelerated plasma electrons, will be randomly distributed.

This appears under the condition $\alpha \ll 1$. In this range, denominated as "incoherent Thomson scattering", the spectral density function results from scattering by individual

electrons and is therefore uniquely determined by the electron-velocity distribution function. Keeping this in mind, we remember that the scattered energy flux at the detector is given by the time-averaged real part of the Poynting vector :

$$S_s = c\varepsilon_0 |\mathbf{E}_s|^2, \tag{2.27}$$

where the scattered field strength $\mathbf{E}_s$ is determined by summation over all particles i :

$$\mathbf{E}_s = \sum_i \mathbf{E}_s^i. \tag{2.28}$$

This leads to :

$$\begin{aligned} |\mathbf{E}_s|^2 &= \sum_i \sum_j \mathbf{E}_s^i \cdot \mathbf{E}_s^j \\ &= \sum_i |\mathbf{E}_s^i|^2 + \sum_{\substack{i \\ i \neq j}} \sum_j \mathbf{E}_s^i \cdot \mathbf{E}_s^j. \end{aligned} \tag{2.29}$$

In the case $\alpha \ll 1$ the phases of the separate scattered fields are distributed randomly and the sum over the cross products will vanish. Equation (2.26) shows that the Debye length gets larger, either when the temperature increases or the electron density decreases. For the TORTUR tokamak ($T_e \leq 1keV, n_e \leq 10^{20}m^{-3}$) the Debye length is in the order of 10 micrometers. By using a laser in the visible light region, α will be in the order of 10^{-2} (for 90° scattering). So, in this case the scattering mechanism is described by incoherent Thomson scattering and the experimental results will be unambiguously related to the electron-velocity distribution.

In the scattering region $\alpha \gg 1$ the spectrum is governed by the collective behaviour of the electrons and is named "coherent scattering" or "collective scattering". In the TORTUR tokamak density fluctuations are measured by means of small-angle and 90° scattering of a 2 mm beam launched in the plasma. When the plasma parameter $\alpha \simeq 1$ the spectral profile will result from both the individual velocities and collective behaviour (plasma waves) of the electrons.

We have seen, that in the case of Thomson scattering, the power scattered by a plasma is obtained simply by adding the powers of the individual electrons. Accordingly, the total scattering cross section $\sigma_T(\lambda_s, \theta_s)$ is obtained by averaging the cross section $\sigma_s(\lambda_s, \theta_s)$ over the electron-velocity distribution function $f(\beta)$. Consequently, for the scattering angle θ_s :

$$\sigma_T(\lambda_s, \theta_s) = \int_0^1 \int_\Omega \sigma_s(\lambda_s, \theta_s) f(\beta) \beta^2 \, d\beta \, d\Omega. \tag{2.30}$$

where $f(\beta)$ is normalized to 1 by :

$$\int_0^1 \int_\Omega f(\beta) \beta^2 \, d\beta \, d\Omega = 1. \tag{2.31}$$

The angular part of the integration (2.30) has been performed by Zhuravlev and Petrov (1972) assuming an isotropic velocity distribution function. The integration over Ω leads to an one-dimensional integral over β :

$$\sigma_T(\lambda_s, \theta_s) = \frac{2\pi r_0^2 \omega^4}{\lambda_i \sqrt{1 - 2\omega \cos\theta_s + \omega^2}} \int_{|\beta_{min}(\omega)|}^{1} \gamma^{-2} \beta f(\beta)\, d\beta, \tag{2.32}$$

with $\beta_{min}(\omega)$ given by :

$$\beta_{min}(\omega) = \frac{1 - \omega}{\sqrt{1 - 2\omega \cos\theta_s + \omega^2}}, \tag{2.33}$$

and $\omega = \omega_s/\omega_i$. Electrons with a speed lower than $\beta_{min}(\omega)$ will not contribute to the cross section at ω.

II.3 Scattered spectrum for a relativistic Maxwellian

The Maxwell-Boltzmann distribution is the velocity distribution for a plasma in kinetic equilibrium. Therefore, in the common case, the velocity distribution of the plasma electrons is described by a Maxwellian distribution function. Considering a hot plasma, we will use a relativistic Maxwellian. That can be written as :

$$f(\beta) = C\gamma^5 \exp -[2\frac{c^2}{a^2}\gamma], \tag{2.34}$$

where $a = \sqrt{2kT_e/m_0}$ is the thermal speed and the normalization constant C is such that equation (2.31) is satisfied.

$$C = \frac{c^2/a^2}{2\pi K_2(2c^2/a^2)}, \tag{2.35}$$

where K_2 is the modified Bessel function of the second kind of order two. The Bessel function can be expanded in an asymptotic series in powers of a^2/c^2 :

$$K_2(2c^2/a^2) \sim \frac{\sqrt{\pi}}{2}\frac{a}{c} e^{-2c^2/a^2} X(a/c), \tag{2.36}$$

with

$$X(a/c) \cong 1 + \frac{15}{16}\frac{a^2}{c^2} + \frac{105}{512}\frac{a^4}{c^4}. \tag{2.37}$$

The relativistic Maxwellian is an isotropic distribution function and is completely determined by the temperature of the plasma electrons.

Mattioli (1974) has obtained an analytical expression for the scattered spectrum for a relativistic Maxwellian.

$$\sigma_T(\lambda_s, \theta_s) = \sigma_{T0} Y(\omega) \exp -\frac{c^2}{a^2} Z(\omega), \tag{2.38}$$

Fig.2.2 Spectral density function for a relativistic Maxwellian for a 90° scattering arrangement (polarization $\mathbf{e}_i$ of the incident e.m. wave normal to the scattering plane, scattered light passed through a polarizer as described).

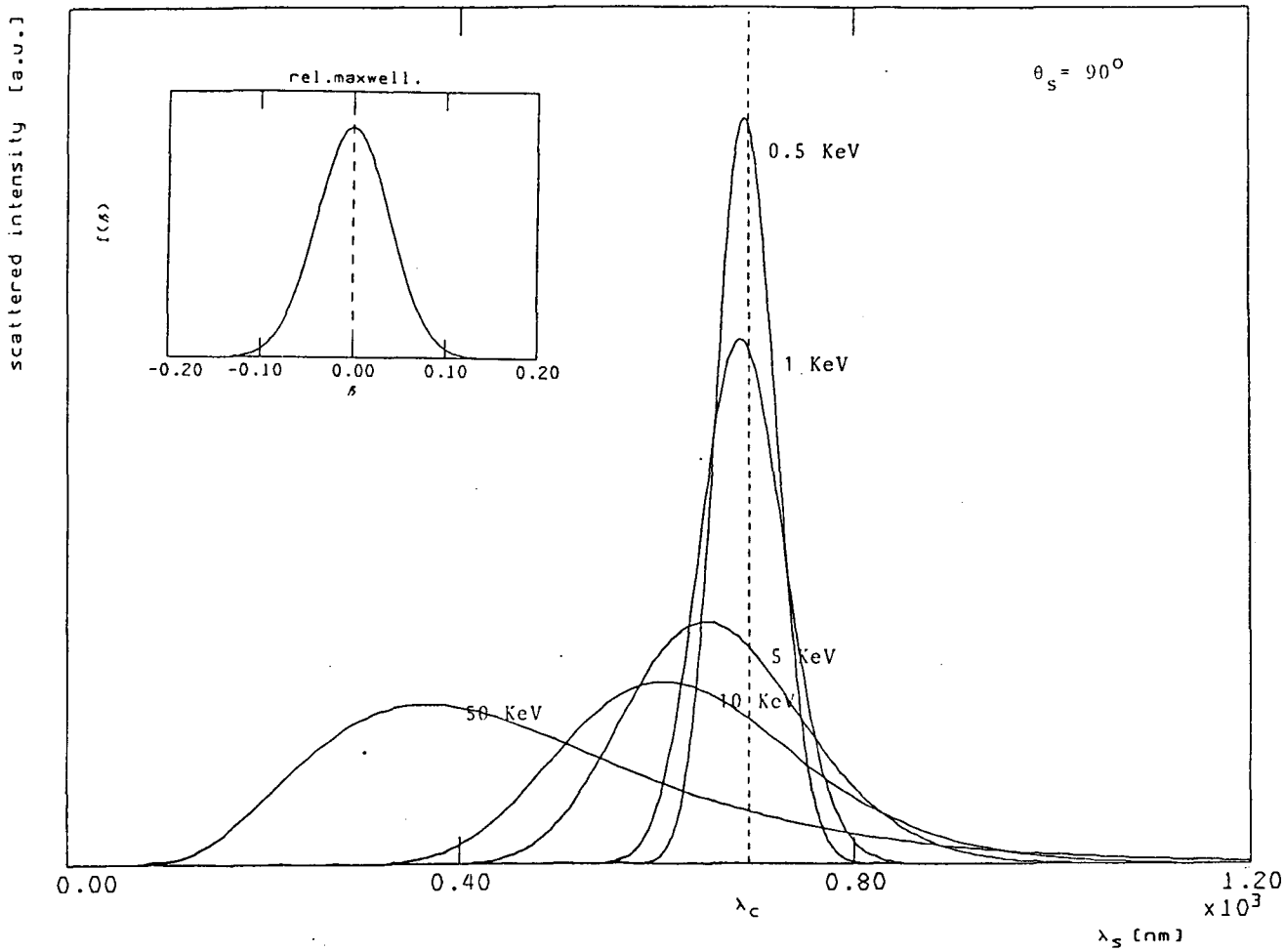

Fig.2.3 Spectral density function for a 5keV relativistic Maxwellian for different angles θ_s between the incident wave vector $\mathbf{k}_i$ and the scattered wave vector $\mathbf{k}_s$.

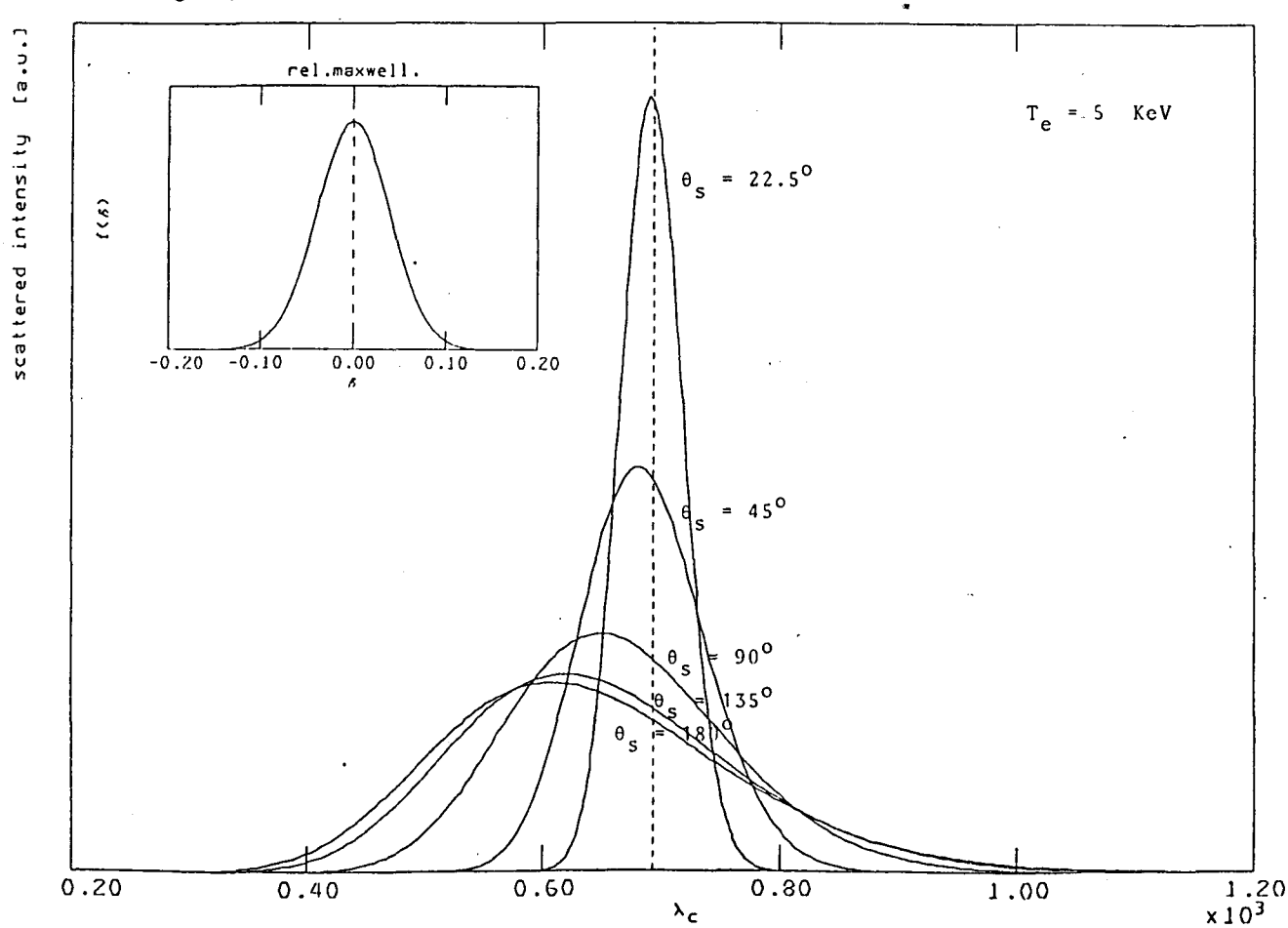

where σ_{T0}, $Y(\omega)$ and $Z(\omega)$ are :

$$\sigma_{T0} = \frac{r_0^2}{2\lambda_i\sqrt{\pi}\sin\theta_s/2}\frac{c}{a}X(a/c)^{-1}, \tag{2.39}$$

$$Y(\omega) = \frac{2\omega^4\sin\theta_s/2}{\sqrt{1-2\omega\cos\theta_s+\omega^2}}, \tag{2.40}$$

and

$$Z(\omega) = \left[\frac{\sqrt{\omega^{-1}-2\cos\theta_s+\omega}}{\sin\theta_s/2} - 2\right] \tag{2.41}$$

(note that $Z(\omega) = 0$ and $Y(\omega) = 1$ for $\omega = 1$).

The scattered spectra are non-symmetrical with respect to the central wavelength. This is shown in *Fig. 2.2*, where we have plotted for the ruby laser wavelength the scattered power as a function of the scattered wavelength λ_s for several temperatures. The relativistic effects perturb the spectral profile of the light scattered by the electrons. As a result, the peak appears to be shifted towards the blue. For example, for a temperature of $3keV$, the shift of the scattered line centre ($\approx 32nm$) exceeds 20 % of the total width at half maximum ($\approx 155nm$). As the temperature increases, this shift becomes more important. In *Fig.2.3* the Thomson spectra for a $5keV$ relativistic Maxwellian for different scattering angles are shown. For small scattering angles both the spectral width and the blue shift decreas.

Let us pause for a moment and look at what has been achieved. Applying the methods used by Mattioli, we have derived an integral-expression for the incoherent Thomson spectrum for an arbitrary isotropic distribution function. Evaluation of the integral should be performed numerically by integration over the magnitude of the normalized velocity β. However, in the case of a relativistic Maxwellian distribution function, an analytical expression is obtained for the scattered spectrum. By means of this expression (2.38) our computer code, which is based on equation (2.32), can be checked.

This code offers the opportunity to calculate the scattered spectrum for several kinds of isotropic distribution functions, like :

(1) relativistic Maxwellian	f_{eq};
(2) relativistic Maxwellian with dips	f_{dip};
(3) square function	f_{square}.

As said, in equilibrium, a Maxwellian distribution is used for describing the plasma. The Maxwellian with dips is related to the unperturbed relativistic Maxwellian (f_{eq}) by :

$$f_{dip}(\beta) = \begin{cases} c_1 f_{eq}(\beta), & \text{if } \beta_{min1} \le \beta \le \beta_{max1}; \\ c_2 f_{eq}(\beta), & \text{if } \beta_{min2} \le \beta \le \beta_{max2}; \\ \ldots & \\ c_I f_{eq}(\beta), & \text{if } \beta_{minI} \le \beta \le \beta_{maxI}; \\ f_{eq}(\beta), & \text{elsewhere.} \end{cases} \tag{2.42}$$

Fig. 2.4 Spectral density function for 90° scattering for a 800eV Maxwellian with a dip.

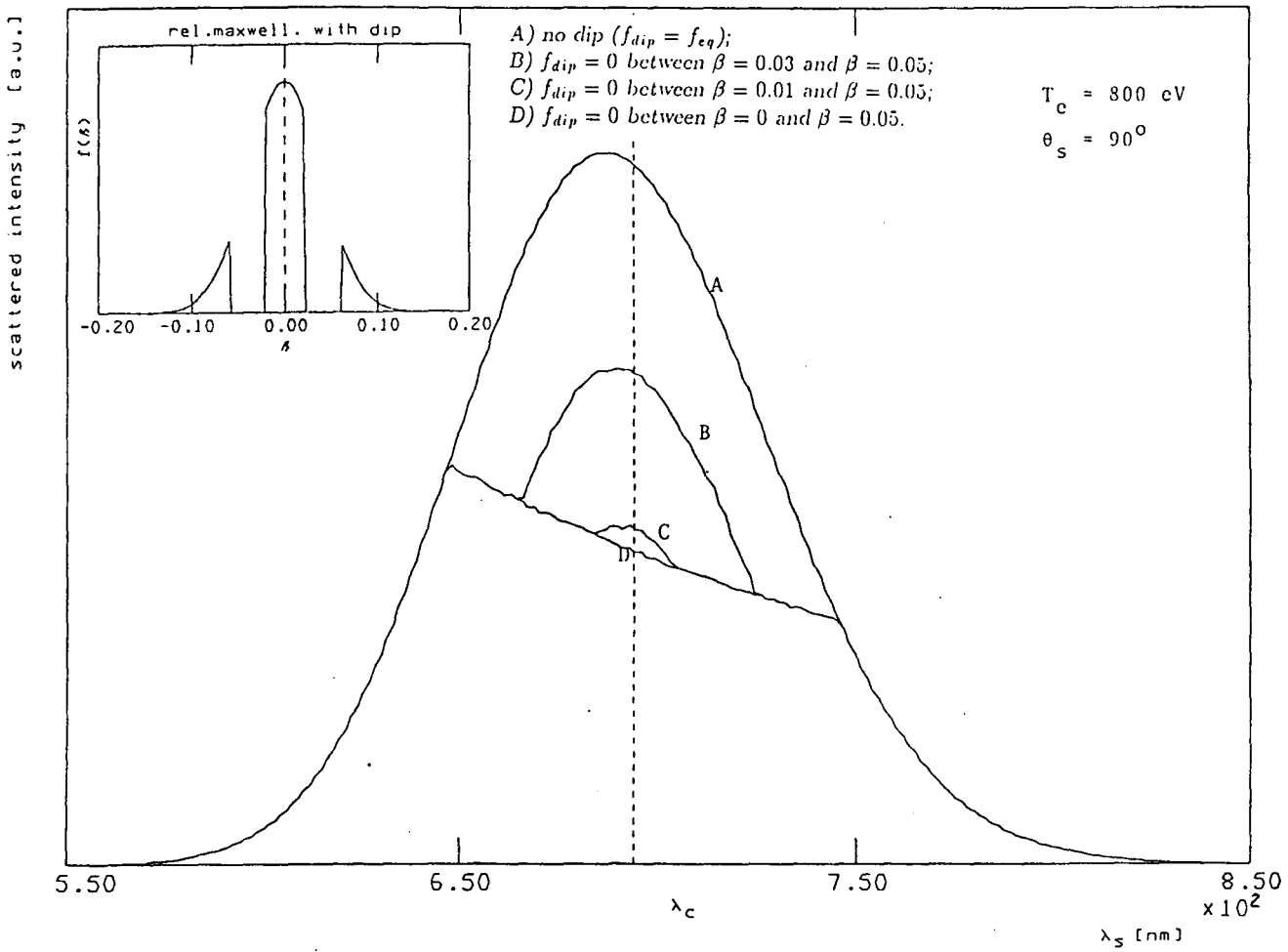

Fig. 2.5 Spectral density function for 90° scattering for a square electron velocity distribution function ($\beta_{min} = 0$ and $\beta_{max} = \beta$).

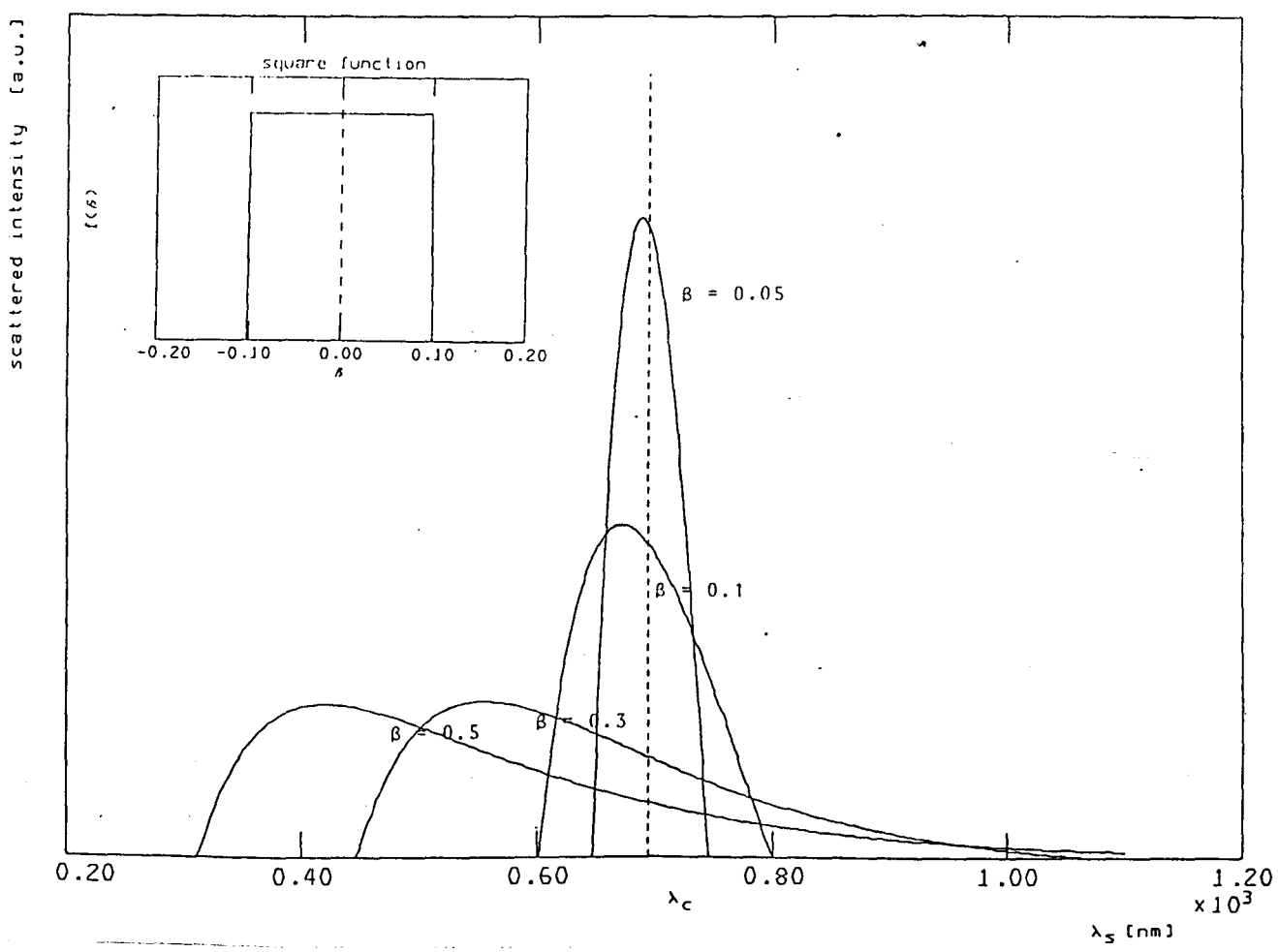

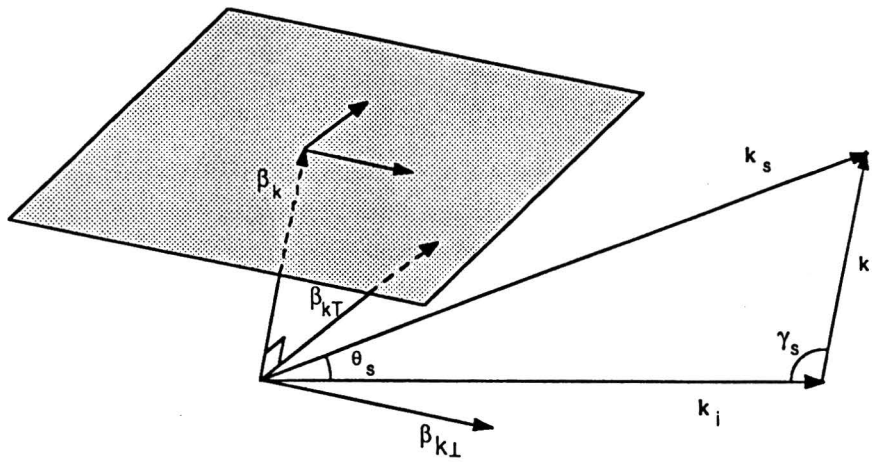

Fig.3.1 *Relation between the* $(\beta_k, \beta_{k\perp}, \beta_{kT})$ *and* $(\beta_i, \beta_s, \beta_E)$ *coordinate system.*

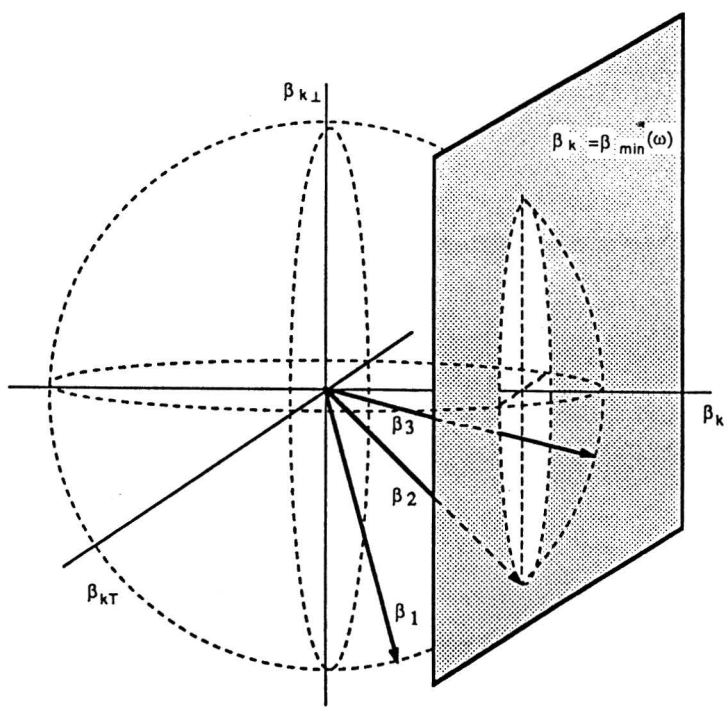

Fig.3.2 *Electrons that have the same velocity component along* β_k *will be scattered at the same frequency. Calculating the scattered intensity at the frequency* ω *will involve an integration in velocity space over a plane, which is defined by* $\beta_k = \beta_{min}(\omega)$. *The velocity* β_1 (β_3) *will not contribute to the cross section at* ω, *because the projected velocity* β_{k1} (β_{k3}) *is to small (large).*

The region $\beta_{minI} \leq \beta \leq \beta_{maxI}$ defines a spherical shell in velocity space. So, by taking f_{dip} we can scan the velocity space and investigate the way in wich some parts of the velocity space influence the scattered spectrum. In *Fig. 2.4* we have plotted the calculated spectra for a Maxwelian distribution with one dip ($c_1 = 0$). When no electrons are present with velocities smaller than β_{max1} the spectrum is characterized by an almost straight line between the points in the spectrum corresponding to β_{max1}. The negative slope of this line again emphasizes the asymmetry of the spectrum due to relativistic effects. The areas between the different spectra represent the intensity scattered by electrons, having their velocities within the corresponding spherical shell.

The square function is defined by :

$$f_{square}(\beta) = \begin{cases} h, & \text{if } \beta_{min} \leq \beta \leq \beta_{max}; \\ 0, & \text{elsewhere,} \end{cases} \tag{2.43}$$

where $h = [\frac{4}{3}\pi(\beta_{max}^3 - \beta_{min}^3)]^{-1}$. This value follows from the normalization condition, equation (2.31). The calculated spectra are shown in *Fig.2.5*. For small values of β_{max} the scattered spectrum has a parabolical form. By increasing this parameter the spectrum will be deformed because of relativistic effects.

Herewith, we have set a solid basis for calculating the Thomson spectra for an arbitrary non-isotropic distribution function. This will be treated in the following chapter.

III.Scattered spectra for an anisotropic electron-velocity distribution function

In this chapter we will describe the computation of the Thomson spectrum for an arbitrary electron velocity distribution. The method we will follow is founded on an article by Matoba *et al.* (1979).

Matoba's approach is encouraged by the fact that the delta function δ, which appears in equation (2.24), picks out those electrons with just the right velocity in the direction of the scattering vector $\mathbf{k}$. This is demonstrated mathematically by the next derivation.

Recalling that the delta function δ is zero everywhere except in case :

$$\omega = \frac{\omega_s}{\omega_i} = \frac{(1-\beta_i)}{(1-\beta_s)}, \tag{3.1}$$

where it goes to infinity in a manner so to encompass a unit area. We may rewrite condition (3.1) as follows :

$$\begin{aligned} \omega_s - \omega_i &= \omega_s\beta_s - \omega_i\beta_i \\ &= (\mathbf{k}_s - \mathbf{k}_i)\cdot\boldsymbol{\beta}c \\ &= k\beta_k c, \end{aligned} \tag{3.2}$$

where β_k is the velocity along the scattering vector $\mathbf{k}$. The delta function thus becomes :

$$\delta\left(\beta_k - \frac{\omega_s - \omega_i}{kc}\right). \tag{3.3}$$

The delta function set down in this way incites the use of an appropiate coordinate system in velocity space to obtain the total cross section $\sigma_T(\lambda_s, \theta_s)$ by integrating the individual cross sections $\sigma_s(\lambda_s, \theta_s)$ over the electron-velocity distribution function.

An obvious choice of coordinates is $(\beta_k, \beta_{k\perp}, \beta_{kT})$, where β_k, $\beta_{k\perp}$ and β_{kT} are the velocities along the scattering vector, perpendicular to the scattering vector within the plane of the $\mathbf{s}$ and $\mathbf{i}$ vectors, and perpendicular to the plane of $\mathbf{s}$ and $\mathbf{i}$, respectively, as shown in *Fig.3.1.*

$$\beta_k = \hat{\mathbf{k}}\cdot\boldsymbol{\beta}, \quad \beta_{k\perp} = \hat{\mathbf{k}}_\perp\cdot\boldsymbol{\beta} \quad \text{and} \quad \beta_{kT} = \hat{\mathbf{k}}_{kT}\cdot\boldsymbol{\beta}. \tag{3.4}$$

Consequently, averaging the cross section $\sigma_s(\lambda_s, \theta_s)$ over the velocity space, can conveniently be written in the coordinates $(\beta_k, \beta_{k\perp}, \beta_{kT})$ (see equation (2.30)) :

$$\begin{aligned} \sigma_T(\lambda_s, \theta_s) = \int\int\int_0^1 & d\beta_k\, d\beta_{k\perp}\, d\beta_{kT} \\ & \sigma_s(\beta_k, \theta_s) f(\beta_k, \beta_{k\perp}, \beta_{kT}) \quad \delta\left(\beta_k - \frac{\omega_s - \omega_i}{kc}\right)\frac{d\beta_k}{d\lambda_s}. \end{aligned} \tag{3.5}$$

The relation between the coordinate system $(\beta_k, \beta_{k\perp}, \beta_{kT})$ and the one defined in chapter II $(\beta_i, \beta_s, \beta_E)$ is given by the matrix equation :

$$\begin{pmatrix} \beta_i \\ \beta_s \\ \beta_E \end{pmatrix} = \begin{pmatrix} -\cos\gamma_s & \sin\gamma_s & 0 \\ -\cos(\gamma_s+\theta_s) & \sin(\gamma_s+\theta_s) & 0 \\ 0 & 0 & -1 \end{pmatrix} \begin{pmatrix} \beta_k \\ \beta_{k\perp} \\ \beta_{kT} \end{pmatrix}. \tag{3.6}$$

In equation (3.6) γ_s is the angle between $\mathbf{k}_i$ and $\mathbf{k}$. Furthermore, we can derive [Matoba] :

$$\frac{d\beta_k}{d\lambda_s} = \frac{\omega^2}{\lambda_i} \frac{(1+\omega)(1-\cos\theta_s)}{(1-2\omega\cos\theta_s+\omega^2)^{3/2}}. \tag{3.7}$$

We substitute equations (2.24), (3.6) and (3.7) into equation (3.5) and find that the wavelength spectrum of the scattered light is given by :

$$\sigma_T(\lambda_s, \theta_s) =$$

$$r_0^2 \int\int\int_0^1 d\beta_k\, d\beta_{k\perp}\, d\beta_{kT}\, \frac{\omega^2}{\lambda_i} \frac{(1+\omega)(1-\cos\theta_s)}{(1-2\omega\cos\theta_s+\omega^2)^{3/2}} (1-\beta^2)$$

$$\times \frac{[(1+\beta_k\cos\gamma_s - \beta_{k\perp}\sin\gamma_s)\{1+\beta_k\cos(\gamma_s+\theta_s) - \beta_{k\perp}\sin(\gamma_s+\theta_s)\} - (1-\cos\theta_s)\beta_{kT}^2]^2}{\{1+\beta_k\cos(\gamma_s+\theta_s) - \beta_{k\perp}\sin(\gamma_s+\theta_s)\}^5}$$

$$\times f(\beta_k, \beta_{k\perp}, \beta_{kT})\, \delta\left(\beta_k - \frac{\omega-1}{\sqrt{1-2\omega\cos\theta_s+\omega^2}}\right), \tag{3.8}$$

where we have rewritten the delta function using the cosine law :

$$k^2 = k_i^2 - 2k_i k_s \cos\theta_s + k_s^2,$$

$$kc = \sqrt{\omega_i^2 - 2\omega_i\omega_s\cos\theta_s + \omega_s^2}. \tag{3.9}$$

In equation (3.8) the angle γ_s between $\mathbf{k}_i$ and $\mathbf{k}$ depends on the electrons' velocity in the direction of the scattering vector. In our experiment, observations are made at a fixed scattering angle $\theta_s = \pi/2$. This means that the scattered light is collected in the horizontal plane $y = 0$. Therefore, in the following we will only consider the case of 90° scattering. In that case the relation between γ_s and β_k is given by [Williamson and Clarke, 1971]:

$$\gamma_s = \frac{\pi}{4} + \frac{1}{2}\sqrt{2}\beta_k + O(\beta_k)^2. \tag{3.10}$$

For a fixed λ_s, equation (3.8) describes an integration, in a three dimensional velocity space, over a plane, which is defined by constant β_k. Looking at *Fig.3.2*, it becomes clear why $|\beta_{min}(\omega)|$ (eq.2.33) has the same form as the argument of the delta function in equation (3.8). It follows from the fact that the electrons in velocity space, bounded by the sphere with radius $|\beta_{min}(\omega)|$, will never intersect the "interaction" plane.

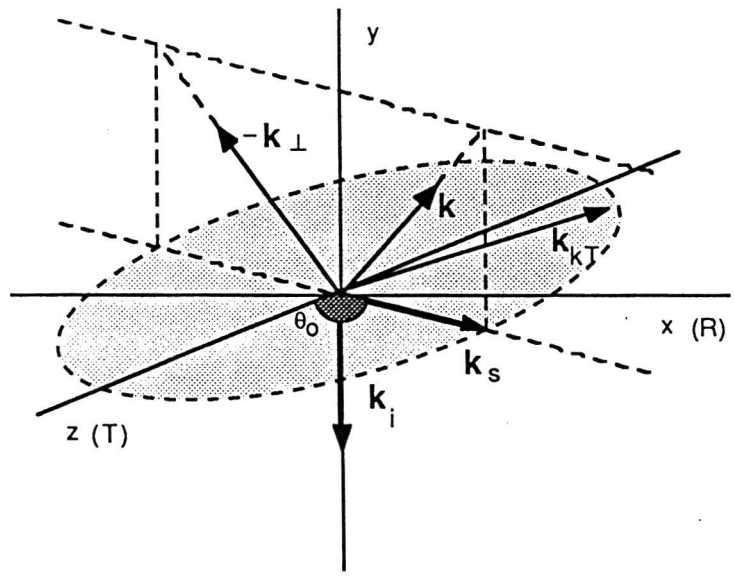

Fig.3.3 Relation between the $(\beta_k, \beta_{k\perp}, \beta_{kT})$ and $(\beta_x, \beta_y, \beta_z)$ coordinate system for 90° scattering. The observation angle θ_o is the angle between the tangential axis and the line of observation. The dotted plane depicts the plane of scattering.

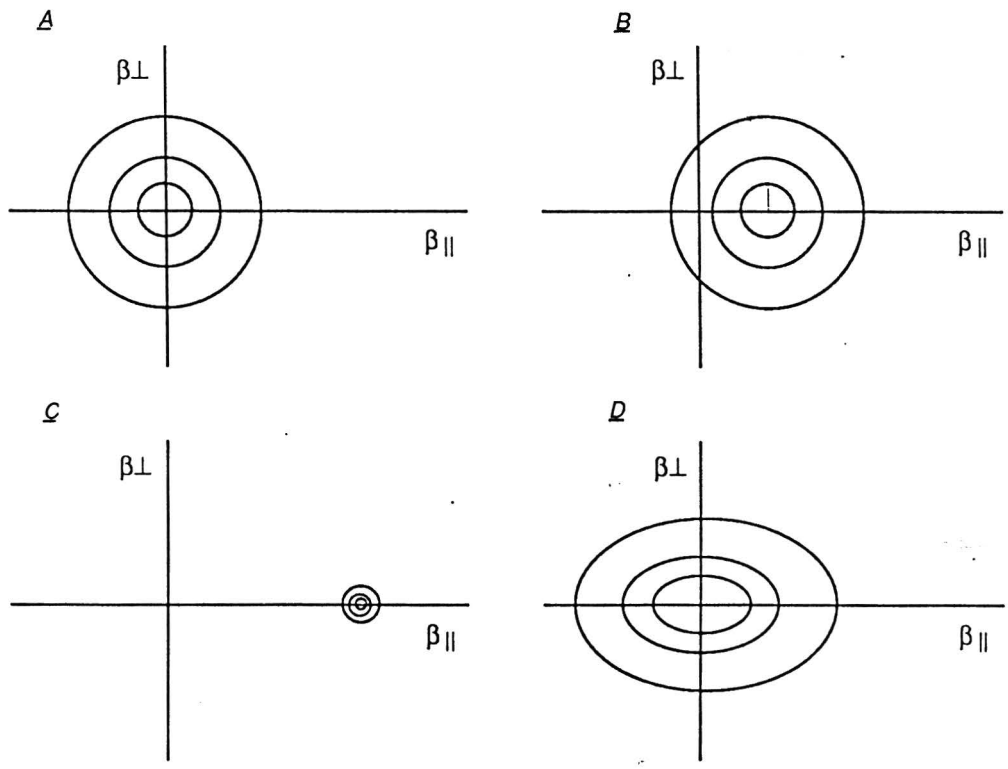

Fig.3.4 Two dimensinal contourplots :
A) contours of constant f for a two dimensional Maxwellian;
B) contours of constant f for a drifting Maxwellian distribution;
C) contours of a beam in two dimensions;
D) contours of constant f for an anisotropic distribution.

Our numerical computations of the scattering cross section per unit wavelength for anisotropic distribution functions are based on equation (3.8).

As a first check, the spectra of the three distribution functions, defined in the former paragraph, are calculated and compared with the ones which have been calculated by means of the integral-expression (2.32). The results of both methods agree within computational errors. Furthermore, we have calculated the scattered spectrum for three kinds of non isotropic distribution functions :

(1) shifted relativistic Maxwellian;
(2) relativistic bi-Maxwellian;
(3) relativistic bobtail distribution.

The properties of these distribution functions will be discussed in the preceding sections.

To keep on line with the experimental set-up and the involved physics, we will define the velocity distribution function $f(\boldsymbol{\beta})$ in the $(\beta_x, \beta_y, \beta_z)$ coordinate system. Here β_x, β_y and β_z are the velocities in radial direction, opposite to the $\mathbf{i}$ vector, and in tangential direction, respectively :

$$\beta_x = \mathbf{x} \cdot \boldsymbol{\beta}, \quad \beta_y = \mathbf{y} \cdot \boldsymbol{\beta} \quad \text{and} \quad \beta_z = \mathbf{z} \cdot \boldsymbol{\beta}. \tag{3.11}$$

For use of $f(\beta_x, \beta_y, \beta_z)$ in the integral expression (3.8), we have to perform a transformation from the scattering coordinates $(k, k_\perp, k_{kT})$ to the (x, y, z)-coordinates. The geometrical relation between the two systems is depicted in *Fig.3.3.* The transformation matrix will be treated in chapter IV.

III.1 Scattered spectra for a shifted relativistic Maxwellian

As mentioned before, the electron-velocity distribution function in thermal equilibrium is given by a Maxwellian distribution, which is of course an isotropic function. In a tokamak plasma, the electrons will have, apart from their thermal motion, a mean directed velocity v_d that corresponds to the local plasma current. The drift velocity is proportional to the local current density j_ϕ :

$$j_\phi = -n_e v_d e. \tag{3.12}$$

In contrast to the total current I_p the j-profile is not easily measured. Tangential Thomson scattering, however, with $\mathbf{k}_s$ parallel to the direction of the plasma current offers the ability to determine the drift velocity v_d. Therefore, as a first choice, we will consider a shifted Maxwellian. The definition of a Maxwellian that is shifted in velocity space over a distance $\boldsymbol{\beta}_d$ is given by :

$$f_{shift} = f_{eq}(\boldsymbol{\beta} - \boldsymbol{\beta}_d), \tag{3.13}$$

where $\boldsymbol{\beta}_d = (\beta_{d_x}, \beta_{d_y}, \beta_{d_z})$.

Three-dimensional anisotropic distribution functions are commonly illustrated with the use of contour maps. The contours are level curves and represent curves of constant $f(\boldsymbol{\beta})$ in velocity space. For example, if the motion is two-dimensional and f is isotropic

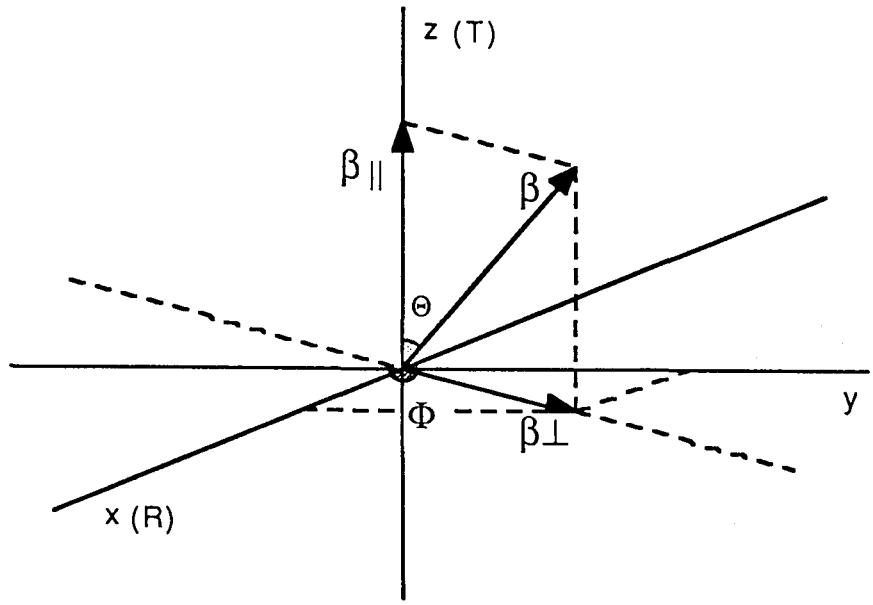

Fig.3.5 Geometrical definition of the polar coordinates (β, θ, ϕ) with respect to the (x, y, z) coordinates. The z axis is defined along the magnetic axis. This means that $\beta_{\|}$ and $\beta_{\perp}$ are the velocities parallel and perpendicular to the magnetic axis, respectively. Notice that in this figure the z axis corresponds to the vertical axis in contrast with the normal way of depicting the z axis in this report, namely as the axis pointed towards the reader!

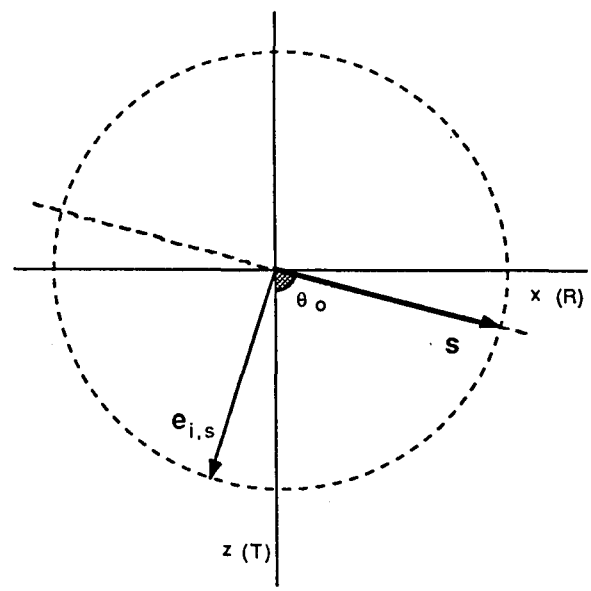

Fig.3.6 Vector orientation of s *and* $\mathbf{e}_{i,s}$ *drawn in the horizontal plane (θ_o = observation angle).*

in $\beta_{\|}$ and $\beta_{\perp}$ the contours of $f(\beta_{\|}, \beta_{\perp})$ will be circles. A drifting Maxwellian would have circular contours displaced from the origin. A beam of particles travelling in any direction would show up as a spike in velocity space. These cases are visualized in *Fig.3.4*

In the experiment, the spectrum is measured in the radial and the tangential direction. Considering also the fact that in most cases a velocity distribution function is chosen symmetric in the magnetic field component we will plot the electron-velocity distribution as a function of $(\beta_{\|}, \beta_{\perp})$, where $\beta_{\|}$ is the velocity parallel and $\beta_{\perp}$ is the velocity perpendicular to toroidal magnetic field B_T, thus :

$$\beta_{\|} = \beta \cos\theta;$$

$$\beta_{\perp} = \beta \sin\theta. \tag{3.14}$$

Furthermore, as shown in *Fig.3.5* :

$$\beta_x = \beta \cos\phi \sin\theta = \beta_{\perp} \cos\phi,$$

$$\beta_y = \beta \sin\phi \sin\theta = \beta_{\perp} \sin\phi \tag{3.15}$$

$$\beta_z = \beta \cos\theta = \beta_{\|}.$$

The latter system is just a polar coordinate system with θ and ϕ the angle between the electrons' velocity $\boldsymbol{\beta}$ and the z axis and the x axis, respectively. Herewith, all coordinate systems which are used in this report have been defined.

III.1.1 Small drift velocities : $\beta_d \leq 0.005$

Since no additional heating is applied in the TORTUR tokamak the drift velocity will be much smaller than the thermal velocity. A rough estimate of the drift velocity can be made by looking at the safety factor $q(r)$, which is proportional to the ratio of the toroidal magnetic field B_T to the poloidal magnetic field B_p :

$$q(r) = \frac{r}{R} \frac{B_T}{B_p(r)}, \tag{3.16}$$

where R is the major radius (see *Fig.1.4*). The poloidal magnetic field, induced by the plasma current $I_p(r)$, is given by :

$$B_p(r) = \frac{\mu_0 I_p(r)}{2\pi r}. \tag{3.17}$$

Assuming a parabolical current density profile $j_\phi(r) = j_\phi(0)(1-(r/a)^2)$ results in $I_p(r) = (\pi/2) r^2 j_\phi(0)$. Connecting these formulas brings up the following relation :

$$j_\phi(0) \approx \frac{4}{q} \frac{B_T}{\mu_0 R}. \tag{3.18}$$

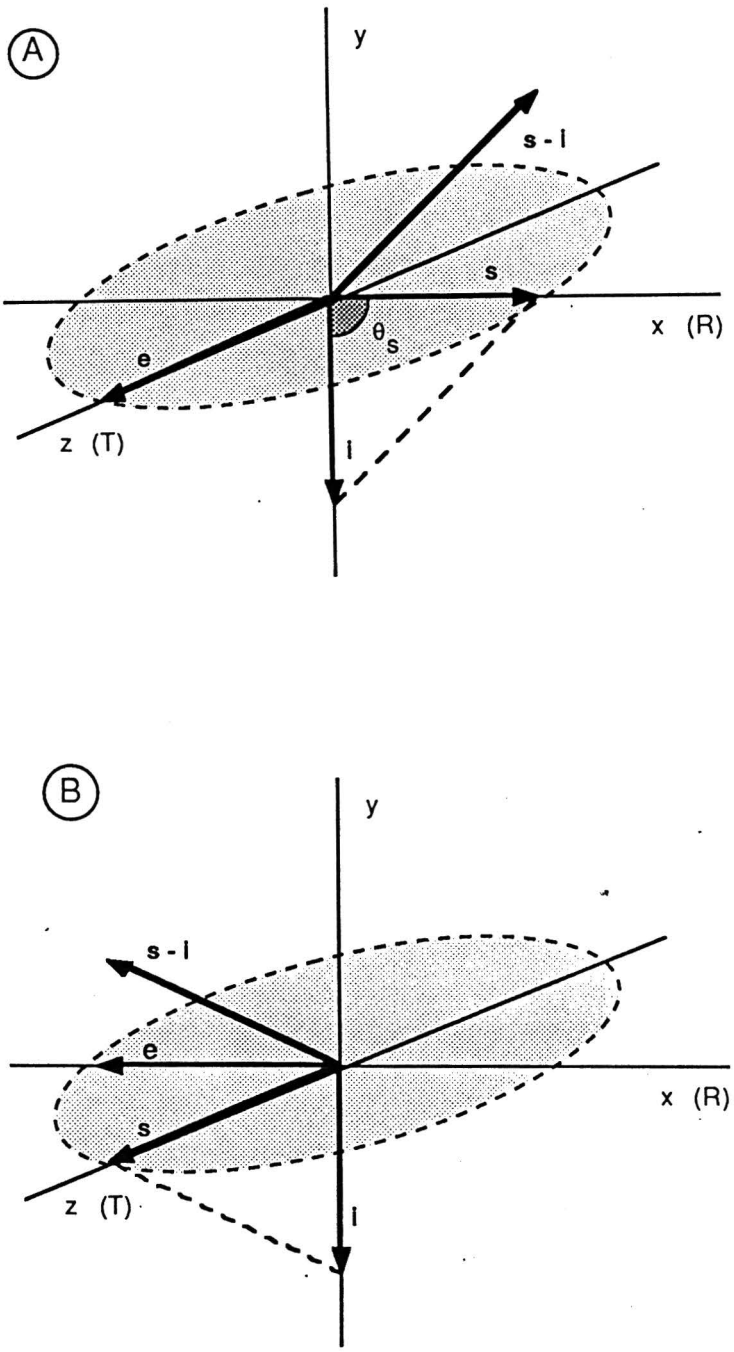

Fig. 3.7 Polarization of the incoming laserlight in case of a) radial and b) tangential scattering.

On account of the Kruskal-Shafranov limit the safety factor must be larger than 1. If the current density is determined by using equation (3.18) this restriction provides an upper limit for the current density.

In the TORTUR tokamak ($R = 0.46m, a = 0.085m, B_T \leq 2.9T, I_p \leq 55kA, T_e \leq 1keV, n_e \leq 10^{20}m^{-3}$) the upper limit for the current density, corresponding to $q = 1$, approximately becomes $j_\phi \approx 2 \cdot 10^7 A/m^2$. With a density $n_e = 6 \cdot 10^{19}m^{-3}$, the drift velocity becomes : $v_d \approx 2 \cdot 10^6 m/s$. Comparing this to the thermal velocity v_{the} when the electron temperature T_e is $800eV$:

$$v_{the}(T_e) = \left(\frac{2kT_e}{m_0}\right)^{1/2} = 5.9 \times 10^5 T_{eV}^{1/2} m/s. \tag{3.19}$$

Thus $v_{the}(800eV) = 1.68 \times 10^7 m/s$ and we see that the ratio v_d/v_{the} indeed is small.

In this case, the tangential spectrum corresponds to a shifted Gaussian spectrum. If the plasma current is pointed towards the observer (positive drift velocity) the spectrum shifts to the blue because of the Doppler shift. A negative drift velocity gives a red shift. The radial spectrum is unaltered by the small drift velocity.

We have calculated the spectrum for a relativistic Maxwellian of $800eV$ ($\beta_{the} = .056$) that is shifted by $v_{d_z} = 7 \cdot 10^5 m/s$ ($\beta_{d_z} = .0023$) in the z direction. The temperature of $800eV$ gives rise to a shift of the scattered line centre of $7.5nm$ towards the blue. The mean directed velocity causes an extra shift of the tangential spectrum of $1.6nm$. The top intensities of the radial and tangential spectra show a minor difference ($< 1\%$).

III.1.2 Large drift velocities : $0.1 \leq \beta_d \leq 0.4$

When a charge is accelerated and observed in a reference frame where its velocity is small compared to the velocity of light, then in that coordinate frame the acceleration field in equation (2.5) reduces to :

$$\mathbf{E}_a = \frac{e}{4\pi\varepsilon_0 c}\left[\frac{\mathbf{s} \times \mathbf{s} \times \dot{\boldsymbol{\beta}}}{R}\right]_{ret}. \tag{3.20}$$

In that case the power radiated per unit solid angle shows a characteristic $\sin^2\theta_s$, where θ_s is measured relative to the direction of acceleration. In the direction of acceleration no light is radiated. Referring to our scattering experiment we notice that by taking the polarization vector of the incident laser light perpendicular to the line of observation a maximum amount of power scattered per unit solid angle is yielded, as stated before.

For observations made in the horizontal plane (90° scattering) at the angle θ_o (o = observer, see *Fig.3.6*) it follows from the geometry :

$$\mathbf{i} = (0, -1, 0), \quad \mathbf{s} = (\sin\theta_o, 0, \cos\theta_o) \quad \text{and} \quad \mathbf{e}_{i,s} = (-\cos\theta_o, 0, \sin\theta_o). \tag{3.21}$$

For example, when the scattered light is observed in the radial direction both the incident and scattered electric fields are polarized along the z direction. In the case of tangential scattering $\mathbf{e}_i$ and $\mathbf{e}_s$ are polarized along the x axis (see *Fig.3.7*).

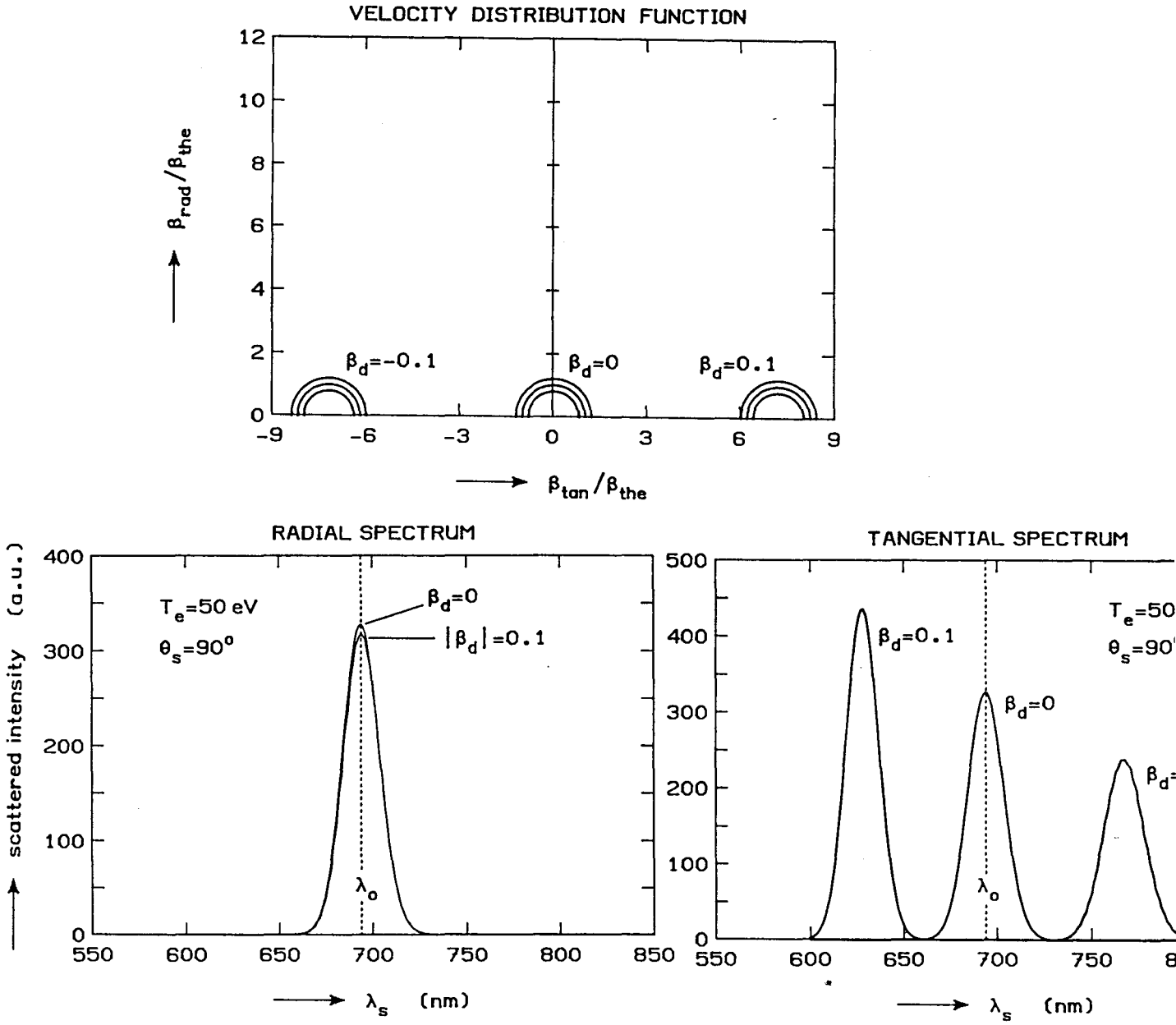

Fig.3.8 Radial and tangential Thomson spectra for shifted 50eV Maxwellians fo different drift velocities $\beta_d = -0.1,\ \ 0,$ and 0.1. along the tangential axis.

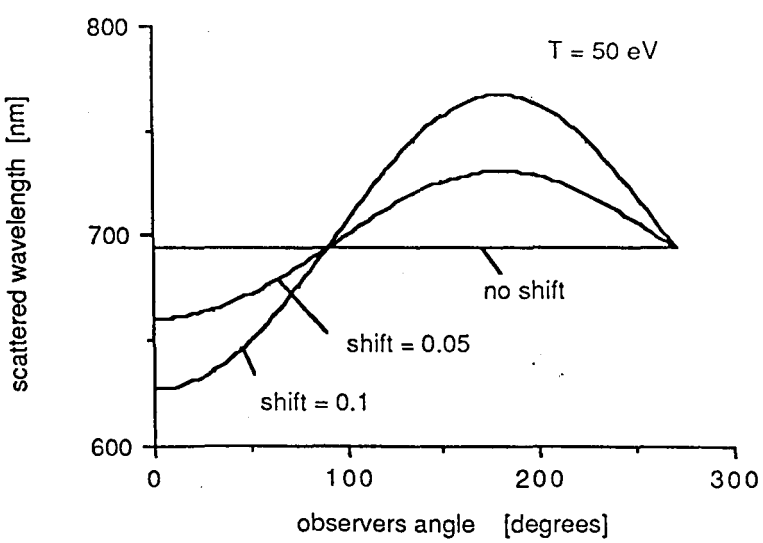

Fig.3.9 Scattered wavelength λ_s as function of the angle of observation θ_o and th drift velocity β_d in the z direction.

For relativistic motion the acceleration fields depend on the velocity as well as the acceleration (equation 2.14). Consequently the angular distribution is more complicated. The acceleration field shows three types of relativistic effects. One is the effect of the specific relationship between the velocity of the electron and its acceleration, which will determine the detailed angular distribution (the factor $(\mathbf{s} \times (\mathbf{s} - \boldsymbol{\beta}) \times \dot{\boldsymbol{\beta}})$). The other is a general, relativistic effect arising from the transformation from the rest frame of the particle to the observers' frame and manifesting itself by the presence of the factor $(1 - \mathbf{s} \cdot \boldsymbol{\beta})^{-3}$. A third factor stems from the mass dependence of the acceleration, which brings up the factor $(1-\beta^2)^{1/2}$. To obtain a better understanding of these high velocity effects, we will consider the special case of a beam of electrons travelling in the z direction, with velocities up to $\beta_{d_z} = 0.4$. The distribution function used is not actually a "beam" but a shifted "low" temperature ($50eV$) Maxwellian. In that case the apparent shift of the spectral peak due to relativistic effects will be of the order of the detection limit of the Thomson-scattering device at TORTUR ($\pm 0.2nm$). So the spectrum of a $50eV$ Maxwellian will roughly be symmetric with respect to the central wavelength. Thus for large drift velocities a "low" temperature Maxwellian can be considered as an electron beam. Calculated spectra for the shifted $50eV$ Maxwellian are shown in *Fig.3.8.*

III.1.2.1 Doppler shift

From the calculated spectra we have plotted the spectral shift $\Delta\lambda = \lambda_s - \lambda_i$ of the peak as function of the drift velocity for observations in the horizontal plane under different angles θ_o to the tangential axis (see *Fig.3.9*).

Let us consider a number of electrons moving in the positive z direction, all having the same velocity $\boldsymbol{\beta} = (0, 0, \beta_{d_z})$. When the light scattered by these electrons is observed at the angle θ_o the projected velocities β_i, β_s and β_E can be derived using equation (2.18) and (3.21) :

$$\beta_i = 0, \quad \beta_s = \beta_{d_z} \cos\theta_o \quad \text{and} \quad \beta_E = \beta_{d_z} \sin\theta_o. \tag{3.22}$$

The Doppler shift caused by the electrons is given by equation (2.12) :

$$\lambda_s = \lambda_i \frac{(1 - \beta_s)}{(1 - \beta_i)}. \tag{3.23}$$

It thus follows from the chosen scattering geometry for the relative Doppler shift $\Delta\lambda/\lambda_i$:

$$\frac{\Delta\lambda}{\lambda_i} = -\beta_{d_z} \cos\theta_o. \tag{3.24}$$

In this case the Doppler shift is only determined by the relative motion of the electron towards the observer. As shown in equation (3.24) the relative Doppler shift is proportional to the electrons' velocity projected to the line of sight.

Fig.3.10 *Peak intensities for an electron beam travelling in the tangential direction with speed β_{d_x}. The top intensities are normalised by the scattered peak intensity for an electron distribution at rest. The scattered intensities are observed at the angle θ_o. The dotted points are top intensities from the calculated spectra.*

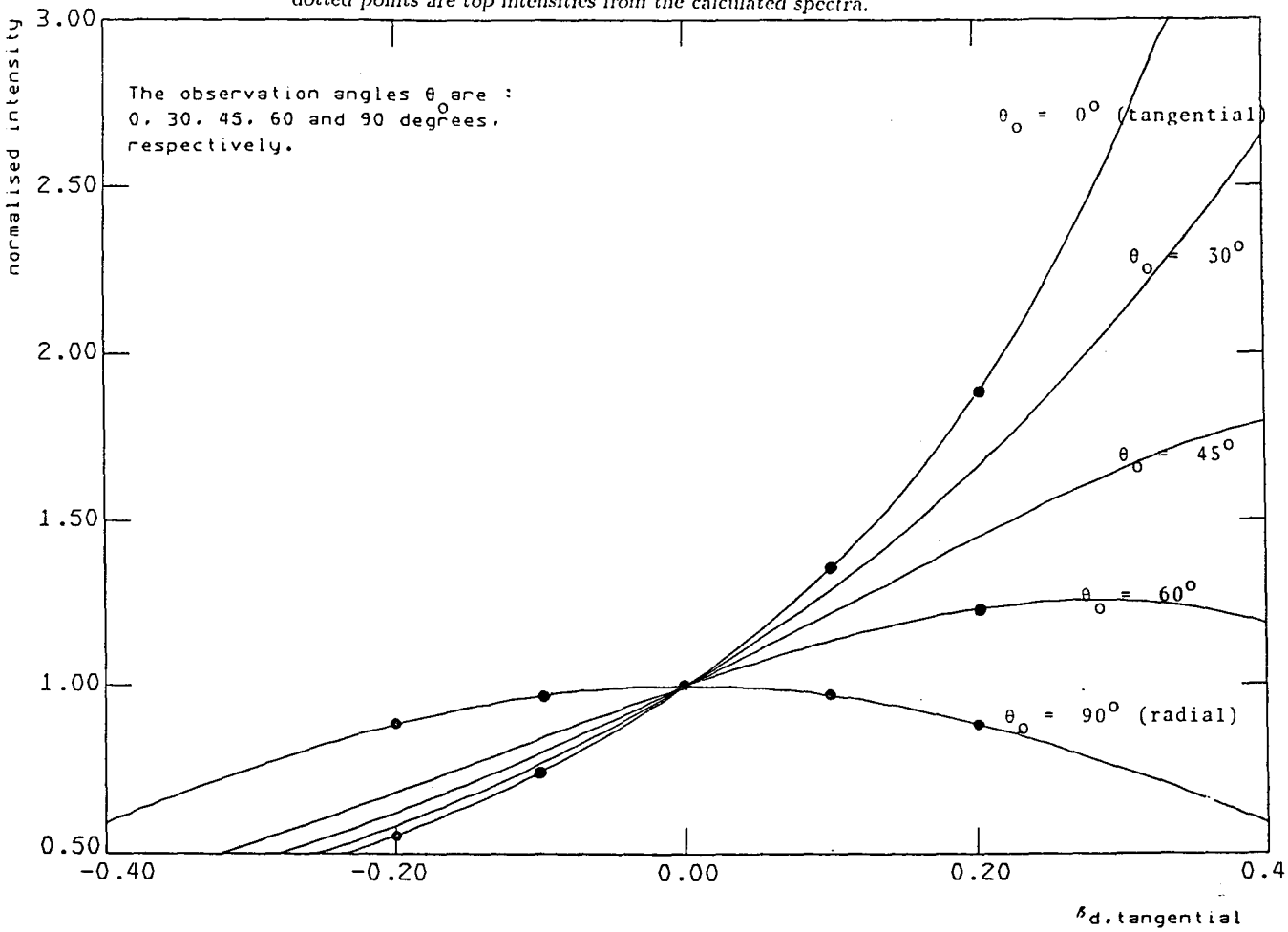

Fig.3.11 *The polar diagram shows the scattered intensities for an electron beam travelling in the tangential direction with speed β_d. The scattered intensities are normalised by the scattered intensity for an electron distribution at rest. In this diagram the distance from the origin represents the normalized scattered intensity and the angle θ defines the angle of observation.*

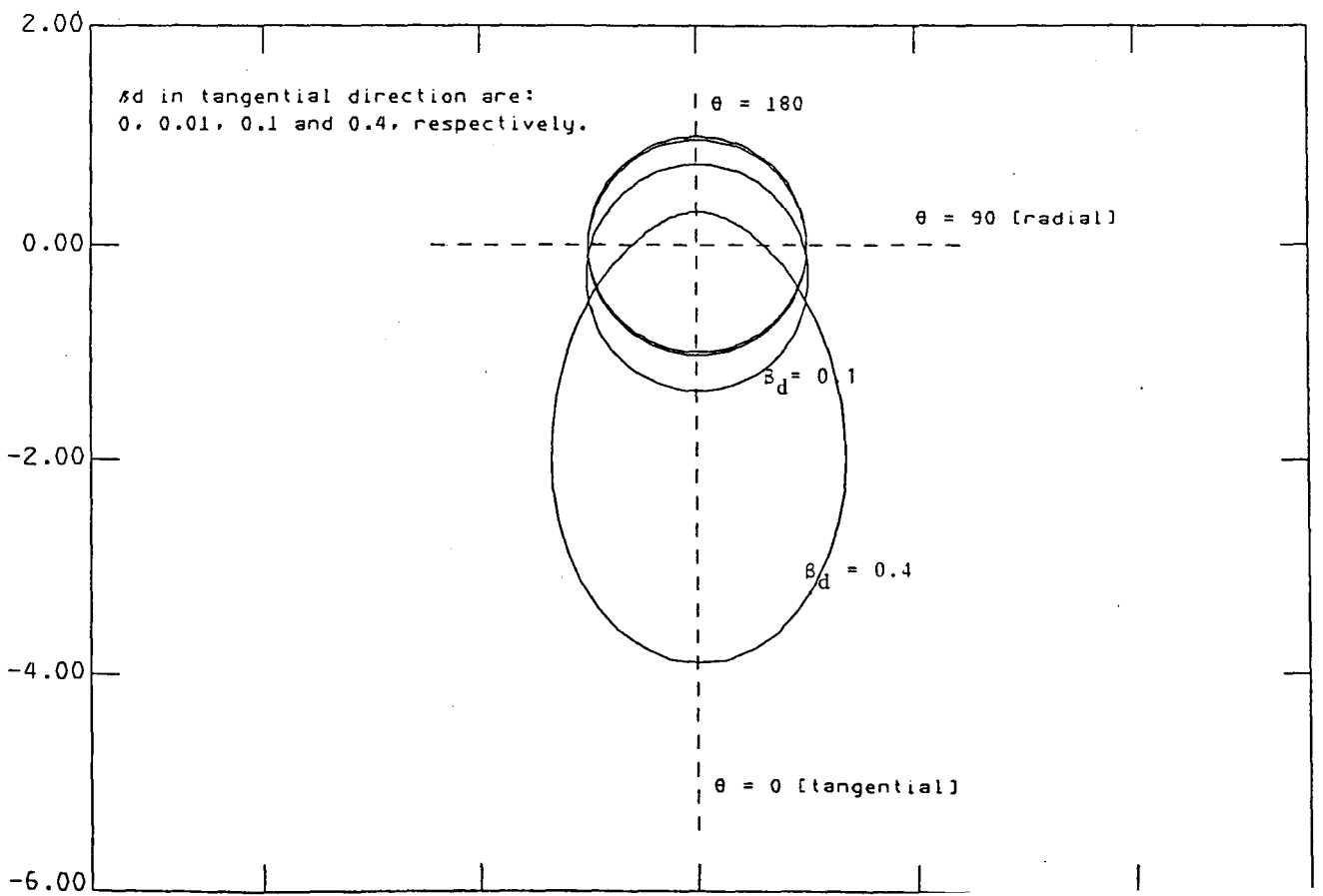

III.1.2.2 Scattered intensities

The peak intensities of the Thomson spectra in *Fig.3.8* show a strong dependence on the drift velocities of the corresponding velocity distribution functions. To comprehend these results we notice that the intensity of the peak is mainly determined by the light that is scattered by electrons moving in the z direction with the specific drift velocity β_{d_z}. For that reason we consider the intensity scattered from a beam of electrons travelling in the z direction at the speed β_{d_z}. Since all the electrons in the beam have the same velocity β_{d_z}, the total cross section is proportional to the cross section for scattering light from a single electron moving with the velocity β_{d_z} in the tangential direction. The scattering cross section per unit wavelength for scattering light from a single electron moving with the speed β is given by equation (2.24). Inserting β_i, β_s and β_E in equation (2.24) displays the scattered intensity from an electron beam travelling in the tangential direction as function of β_{d_z} and θ_o :

$$\sigma_T \propto (1-\beta_{d_z}^2)\left[\frac{1}{(1-\beta_{d_z}\cos\theta_o)^3} - \frac{2\beta_{d_z}^2\sin^2\theta_o}{(1-\beta_{d_z}\cos\theta_o)^4} + \frac{\beta_{d_z}^4\sin^4\theta_o}{(1-\beta_{d_z}\cos\theta_o)^5}\right]. \qquad (3.25)$$

When the radiation is observerved in radial (R) or tangential (T) direction this dependence becomes :

$$\theta_o = \pi/2 \qquad \text{(R):} \qquad \sigma_T \propto (1-\beta_{d_z}^2)^3, \qquad (3.26)$$

$$\theta_o = 0 \qquad \text{(T):} \qquad \sigma_T \propto (1-\beta_{d_z}^2)/(1-\beta_{d_z})^3. \qquad (3.27)$$

The peak intensities of the calculated spectra for different velocity shifts show a same dependence (see *Fig.3.10*). We have plotted the relationship (3.25) in a polar diagram (*Fig.3.11*). We stress that *Fig.3.11* does not pictures the radiation pattern for an accelerated charge.

Remember that, for every direction of observation the incoming and scattered electric field are polarized perpendicularly to the line of sight. In comparing measurements (cq. calculations) at different angles we have to be aware of the fact that the spatial relationship between the velocity of the electron and its acceleration will be different. For radial measurement an electron that moves in the z direction is accelerated by the incoming field nearly parallel to its direction of motion. In case of tangential scattering an electron, moving in the z direction is accelerated nearly perpendicular to its direction of motion. These two cases are depicted in *Fig.3.12*.

It follows from *Fig.3.12* that the polarization of the laser light is chosen so that scattering from an electron at rest yields a maximum amount of power scattered per unit solid angle radiated in the direction of observation. When light is scattered from a moving electron the radiation pattern is stretched out in the direction of motion and the maximum amount of power per unit solid angle is no longer scattered in the direction of observation, at least if the velocity of the electron is not perpendicular to its acceleration.

Thus *Fig.3.12* shows schematically how the radiation pattern from an electron moving in the z direction transforms due to its speed and depending on the direction of the acceleration at the same time. *Fig.3.11* pictures the normalized Thomson cross section

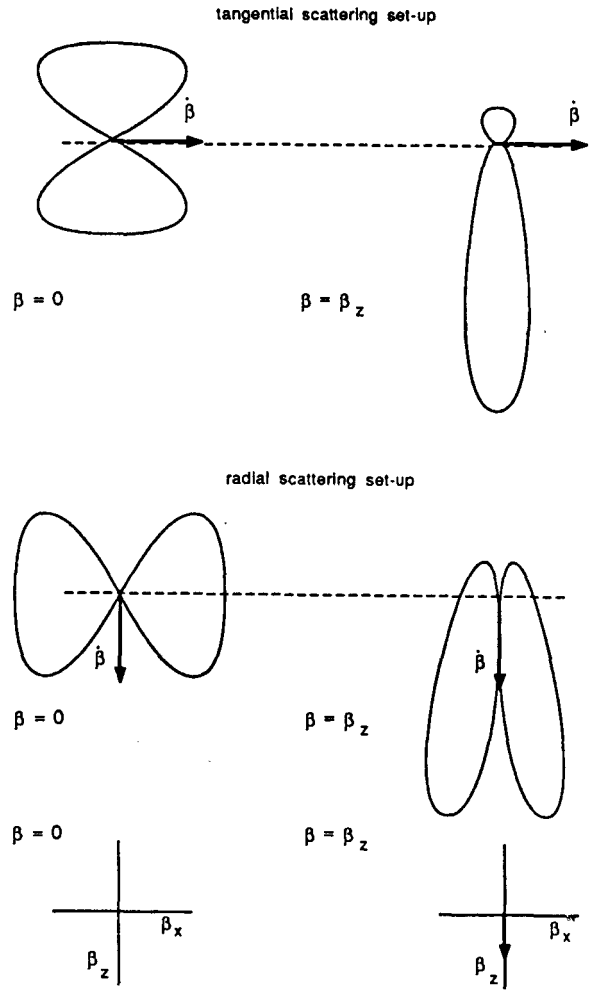

Fig.3.12 Schematic view of the deformation of the radiation pattern for an electron moving in the tangential direction, for a radial ($\mathbf{e}_i \parallel \beta_z$) and tangential ($\mathbf{e}_i \perp \beta_z$) set-up.

for an electron, that moves in the tangential direction, observed under an angle θ_o with the tangential axis. We can conceive the polar diagram in another way by considering the contours as being the intensity scattered from an electron moving in any direction within the horizontal plane measured in the tangential direction. This shows that the extend to which the individual cross sections contribute to the total Thomson cross section depends on the way the individual radiation patterns are transformed. As we have seen, this transformation depends both on the magnitude of the electrons' velocity and the relation between the direction of motion and acceleration. The direction of acceleration is imposed by the experimental (cq. geometical) set-up.

The feature of increasing Thomson-scattering cross section for electrons moving towards the observer likewise causes the blue shift from the central wavelength for the scattered spectrum of a relativistic Maxwellian as shown in *Fig.2.2.* This blue shift thus physically originates from the emission characteristic of an accelerated, relativistic charge.

A last remark, concerning relation (3.25), is connected with a minor question posed at the beginning of our research. When we look at *Fig.1.3*, we see that for tangential measurements the line of observation makes an angle of 4 degrees with the tangential axis. Equation (3.25) shows that deviations from the observed spectrum with the actual tangential spectrum is negligible ($\ll 1\% \approx$ detection limit).

III.2 Scattered spectra for a bi-Maxwellian

In this section we will look at the scattered spectra for a bi-Maxwellian. The reason for taking a bi-Maxwellian distribution function, apart from being analytically simple, is twofold. Firstly, to get an impression of how small a perturbation in velocity space affects the overall shape of spectrum and how it is "seen" by the observer. The latter is done by comparing the radial and tangential spectra. The second reason is related to a statement of Salzmann (1986). He claims : "Thomson scattering is insensitive against small percentages of suprathermal electrons ... even a mono-energetic beam of electrons contributing to a central spectral channel will be undetectable as long as it does not comprise more than $\sim 6\%$ of the electron density ...".

The bi-Maxwellian we consider consists of a $800eV$ relativistic Maxwellian, reffered to as the "bulk", containing 99% of the total electron population, added up by a $5eV$ Maxwellian that is shifted in the horizontal plane (drift velocity $\beta_d = 0.1$). The direction of the shift is determined by the angle between the drift velocity and the tangential axis. The total width at half maximum for a $5eV$ Gaussian spectrum ($\approx 7nm$) is about the size of the spectral bandwidth for the various channels of the polychromator.

Using the bi-Maxwellian, just defined, we can look at the effect the 1% local perturbation has on both the radial and tangential spectrum. *Fig.3.13* shows the calculated spectra for various directions of the distortion as seen by radial and tangential observers. Like in the previous section the velocity of the perturbation electrons is determined by their drift velocities. So, this drift velocity will approximately fix their Doppler shifts.

Furthermore, looking at *Fig.3.13*, we see that, looking at the central region of the radial spectrum, the perturbation contributes to about 3% of the total scattered power, contradicting the statements made earlier by Salzmann.

Fig.3.13a Calculated spectra for a bi-Maxwellian. The perturbation is shifted in the tangential direction (see text in figures).

On this page the calculated spectra for Thomson scattering from an electron velocity distribution, which is modelled by two maxwellians, are plotted. The body is characterised by a temperature of 800 eV. The second maxwellian has a "temperature" of 5 eV. It is shifted in velocity space over a distance 0.1 in tangential direction. The second maxwellian contains 1% of the total electron population and can be considered as a perturbation.

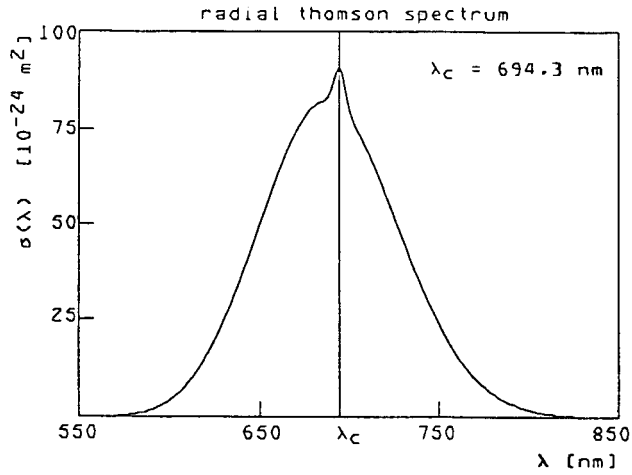

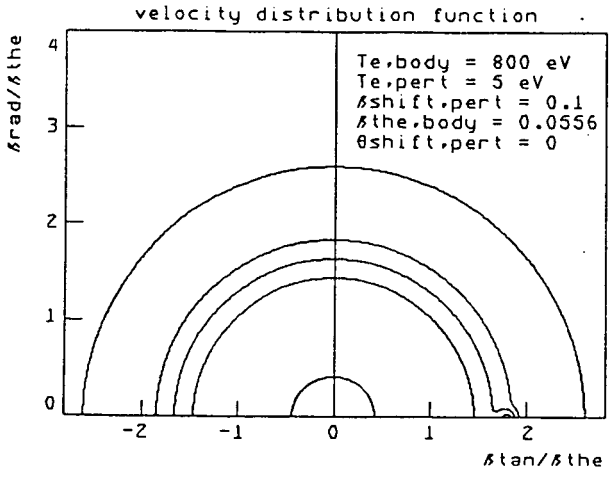

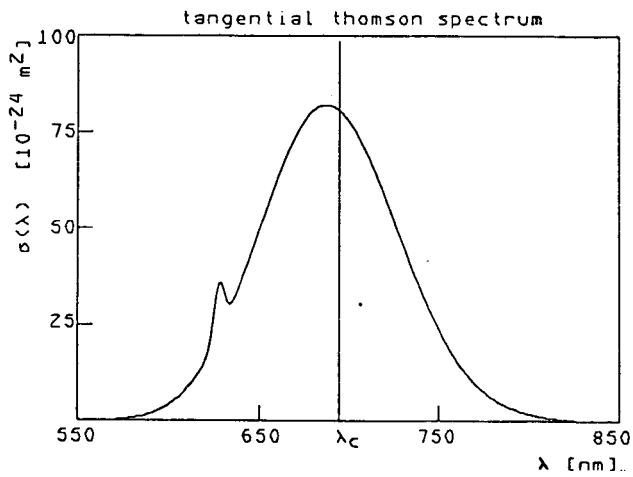

Fig.3.13b Calculated spectra for a bi-Maxwellian (see text in figures).

On this page the calculated spectra for Thomson scattering from an electron velocity distribution, which is modelled by two maxwellians, are plotted. The body is characterised by a temperature of 800 eV. The second maxwellian has a "temperature" of 5 eV. It is shifted in velocity space over a distance 0.1 in the direction that makes a 30 degrees angle with the tangential axis. The second maxwellian contains 1% of the total electron population and can be considered as a perturbation.

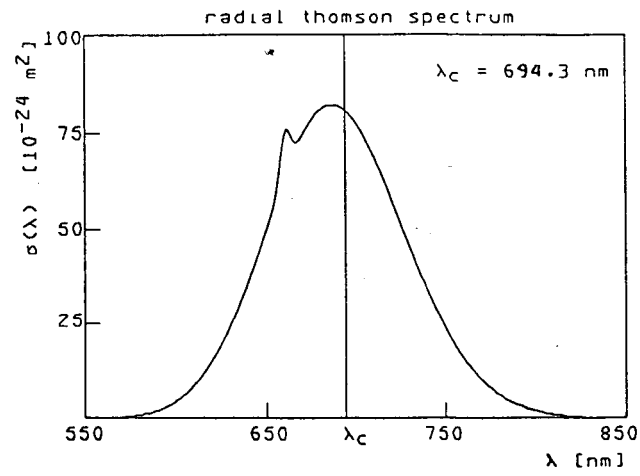

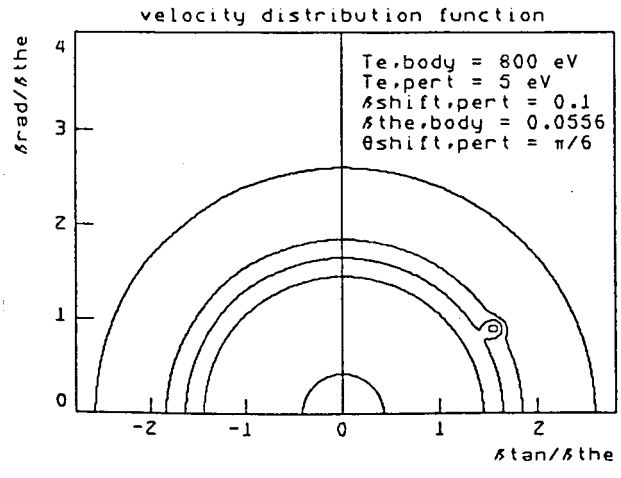

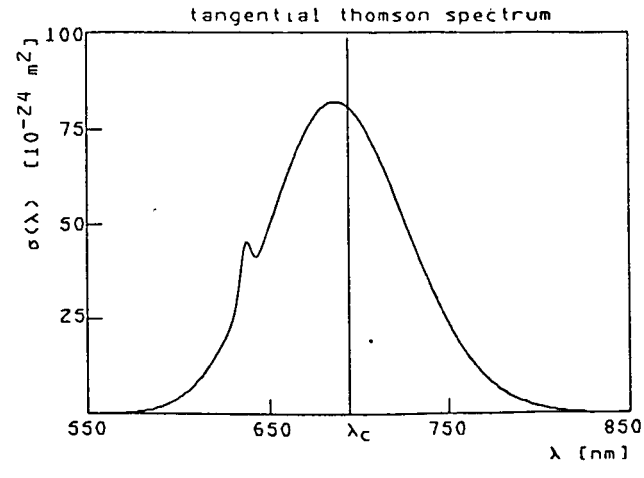

Fig.3.13c Calculated spectra for a bi-Maxwellian (see text in figures).

On this page the calculated spectra for Thomson scattering from an electron velocity distribution, which is modelled by two maxwellians, are plotted. The body is characterised by a temperature of 800 eV. The second maxwellian has a "temperature" of 5 eV. It is shifted in velocity space over a distance 0.1 in the direction that makes a 45 degrees angle with the tangential axis. The second maxwellian contains 1% of the total electron population and can be considered as a perturbation.

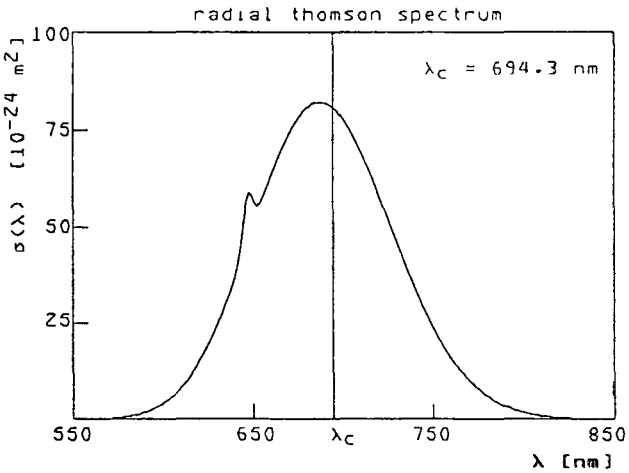

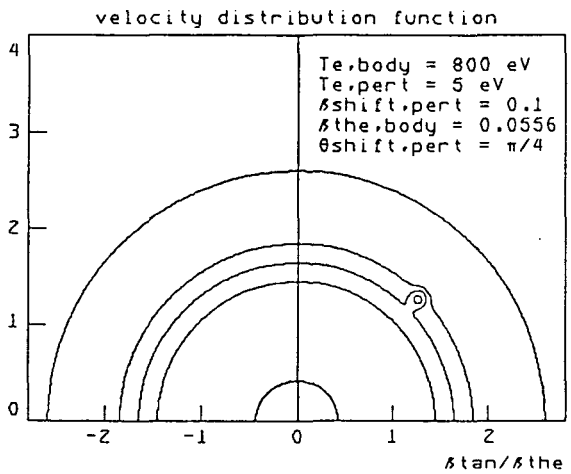

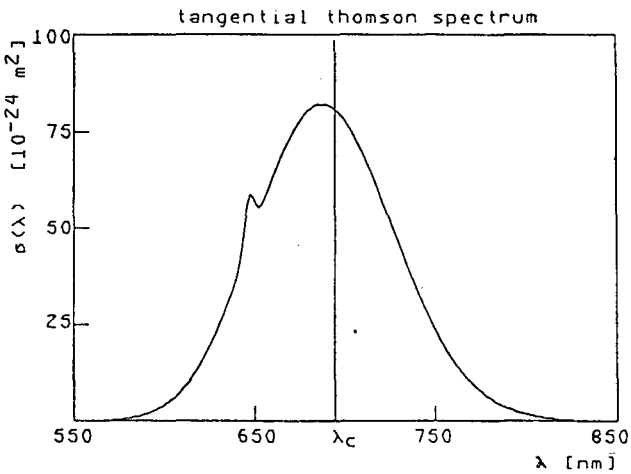

Fig.3.13d Calculated spectra for a bi-Maxwellian (see text in figures).

On this page the calculated spectra for THomson scattering from an electron velocity distribution, which is modelled by two maxwellians, are plotted. The body is characterised by a temperature of 800 eV. The second maxwellian has a "temperature" of 5 eV. It is shifted in velocity space over a distance 0.1 in the direction that makes a 60 degrees angle with the tangential axis. The second maxwellian contains 1% of the total electron population and can be considered as a perturbation.

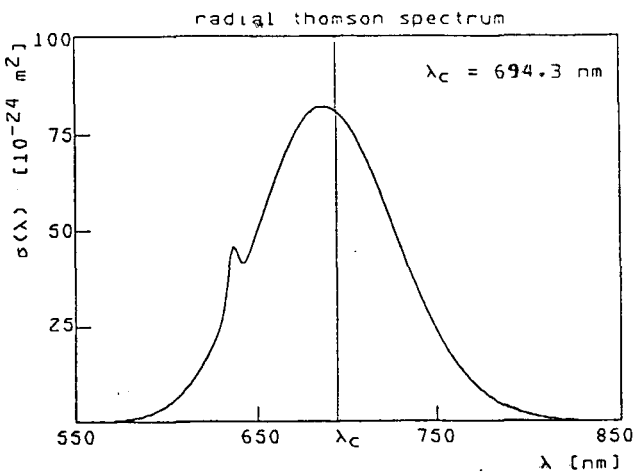

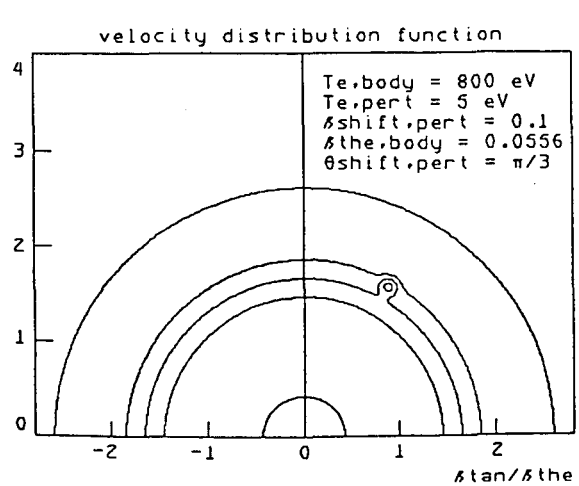

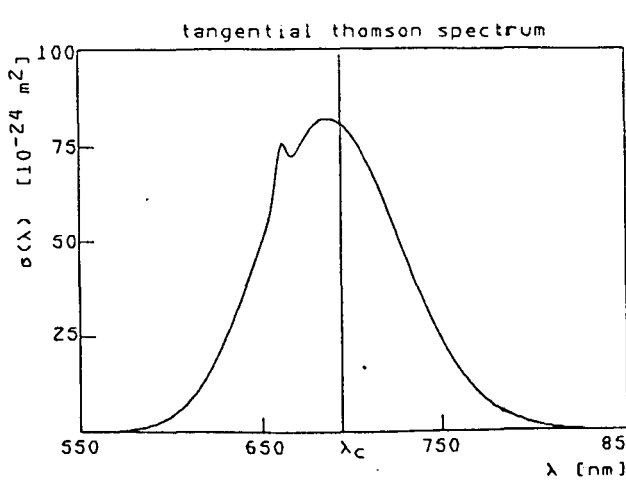

III.3 Scattered spectra for a relativistic bobtail distribution

An electron under the action of a constant electric field will continuously increase its momentum if the driving force of the field overcomes the dynamical friction due to collisions with a background plasma. In a tokamak plasma the electrical field is exerted by the loop voltage V_L.

$$F_{el} = -eV_L/2\pi R. \tag{3.28}$$

The drag force, due to Coulomb interactions with ions and other electrons, can be written as :

$$F_d = m_0 v \nu(v), \tag{3.29}$$

where m_0 is the electron rest mass, v is the electron speed and $\nu(v)$ is the frequency of the Coulomb collisions. The collision frequency falls off strongly if the electron velocity increases :

$$\nu(v) = \frac{e^4 n_e \ln\Lambda}{2\pi\varepsilon_0^2 m_0^2 v^3}, \tag{3.30}$$

where $\ln\Lambda$ is the Coulomb logarithm ($\ln\Lambda \approx 15$ in a tokamak). The critical velocity v_c is defined by balancing the electric field force against the frictional drag of Coulomb collisions :

$$eE = F_d(v_c). \tag{3.31}$$

From equation (3.30) we obtain :

$$v_c^2 = \frac{e^3 n_e \ln\Lambda}{2\pi\varepsilon_0^2 m_0 E}. \tag{3.32}$$

This velocity represents an important cross-over point in the electron-velocity distribution function. Obviously, electrons with velocities $v > v_c$ will be gradualy accelerated by the electric field to high energies. On the other hand, electrons with velocities much lower than v_c will remain in the thermal population. Near the breakpoint $v = v_c$, the electron velocity distribution is gradually transformed from being isotropic to highly directional along the direction of the applied electric field. The critical velocity can be expressed in terms of the critical electric field E_c. This field is given by the following condition :

$$eE_c = F_d(v_{the}), \tag{3.33}$$

which results in :

$$E_c = \frac{e^3 n_e \ln\Lambda}{2\pi\varepsilon_0^2 m_0 v_{the}^2}. \tag{3.34}$$

The significance of E_c is that for fields larger than E_c thermal electrons will run away, whereas when $E < E_c$, only the tail of the distribution is subject to free acceleration. From equations (3.32) and (3.34) it follows that :

$$v_c = v_{the}\sqrt{E_c/E}, \tag{3.35}$$

Fig.3.14a Calculated spectra for a bobtail distribution ($\beta_c = 2\beta_{the}$, see text in figures).

On this page the calculated spectra for the so-called "bobtail" distribution are show n. It is a prototype model for a run-away distribution.
The "bobtail" distribution is formed by a relativistic maxwellian, the body, on which a tail in tangential direction developes after some critical velocity, ßcrit, is exceeded. In the region between ßcrit and ßfin the distribution function takes the value of the maxwellian at ßcrit. In the case represented below the tail roughly contains 2% of the total amount of electrons.

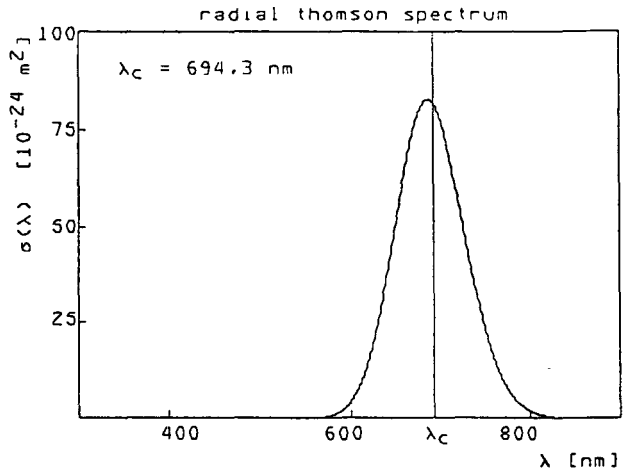

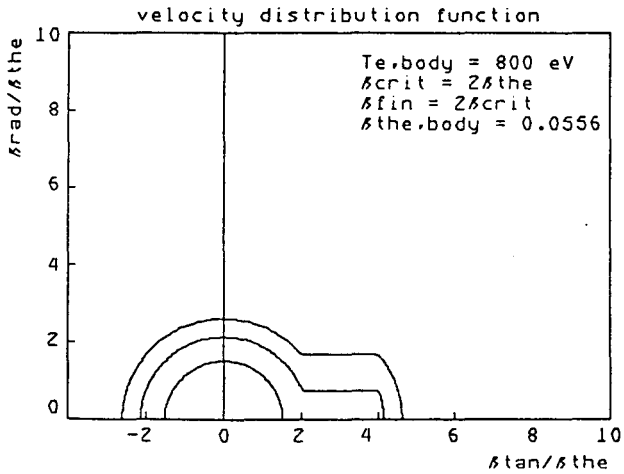

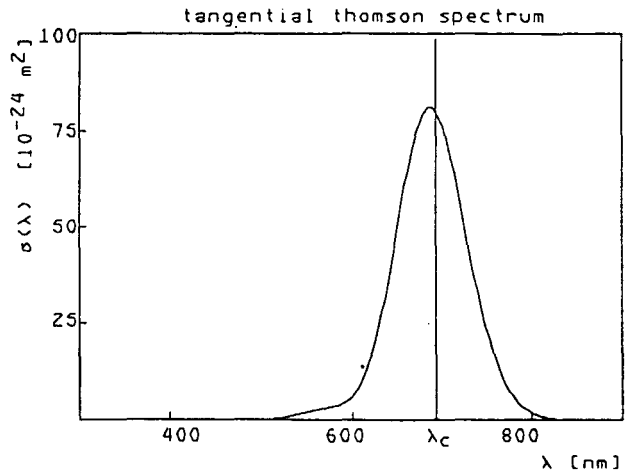

Fig.3.14b Calculated spectra for a bobtail distribution ($\beta_c = 2\beta_{the}$, see text in figures).

On this page the calculated spectra for the so-called "bobtail" distribution are show n. It is a prototype model for a run-away distribution.
The "bobtail" distribution is formed by a relativistic maxwellian, the body, on which a tail in tangential direction developes after some critical velocity, ßcrit, is exceeded. In the region between ßcrit and ßfin the distribution function takes the value of the maxwellian at ßcrit. In the case represented below the tail roughly contains 6% of the total amount of electrons.

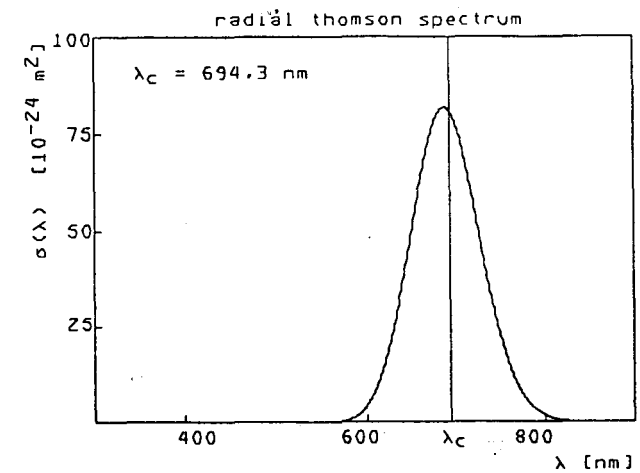

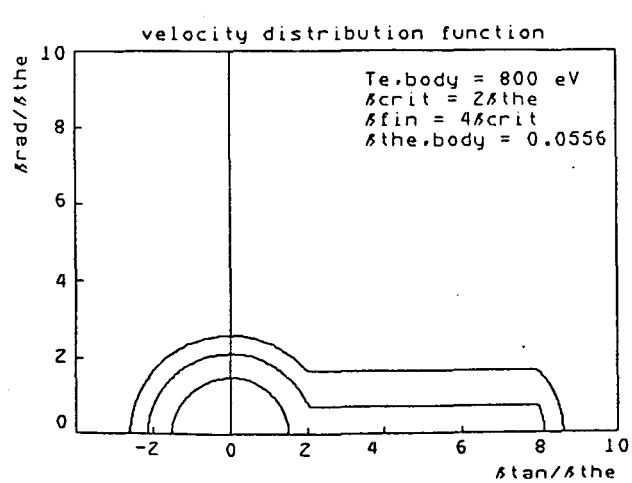

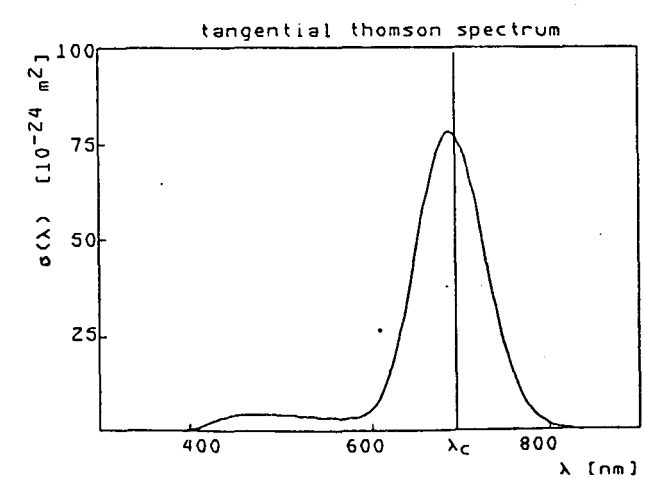

Fig.3.14c Calculated spectra for a bobtail distribution ($\beta_c = \beta_{the}$, see text in figures).

On this page the calculated spectra for the so-called "bobtail" distribution are show n. It is a prototype model for a run-away distribution.
The "bobtail" distribution is formed by a relativistic maxwellian, the body, on which a tail in tangential direction developes after some critical velocity, ßcrit, is exceeded. In the region between ßcrit and ßfin the distribution function takes the value of the maxwellian at ßcrit. In the case represented below the tail roughly contains 17% of the total amount of electrons.

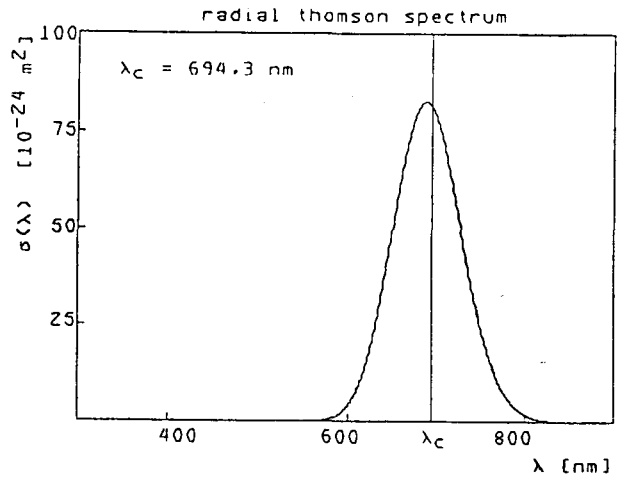

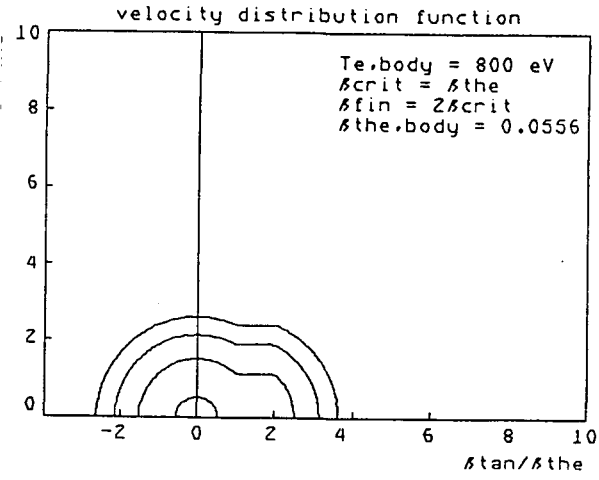

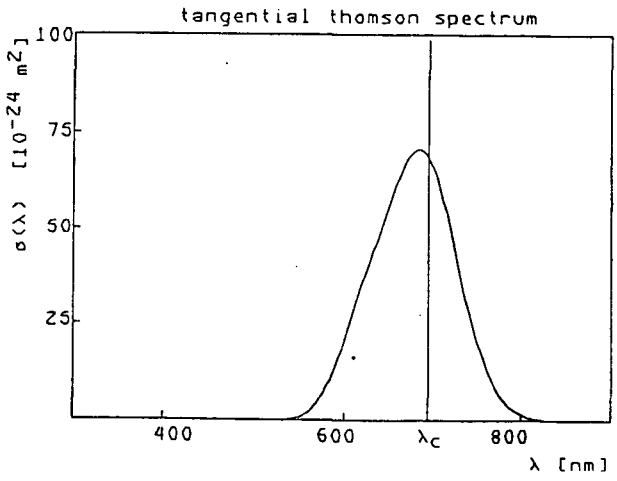

Fig.3.14d Calculated spectra for a bobtail distribution ($\beta_c = \beta_{the}$, see text in figures).

On this page the calculated spectra for the so-called "bobtail" distribution are show n. It is a prototype model for a run-away distribution.
The "bobtail" distribution is formed by a relativistic maxwellian, the body, on which a tail in tangential direction developes after some critical velocity, ßcrit, is exceeded. In the region between ßcrit and ßfin the distribution function takes the value of the maxwellian at ßcrit. In the case represented below the tail roughly contains 38% of the total amount of electrons.

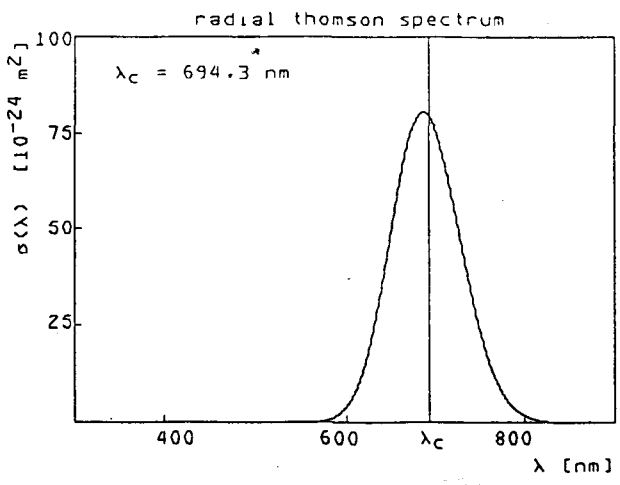

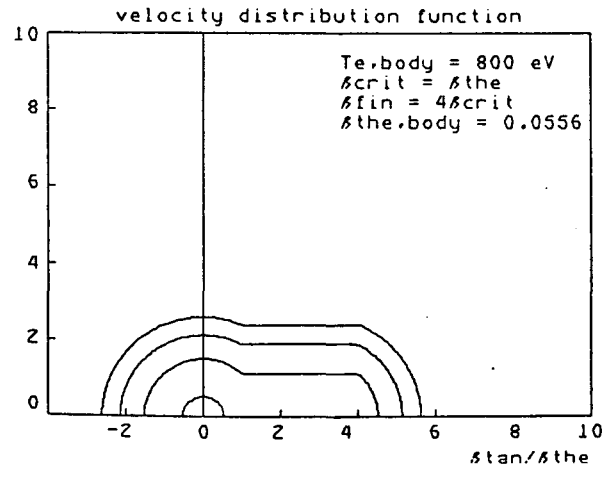

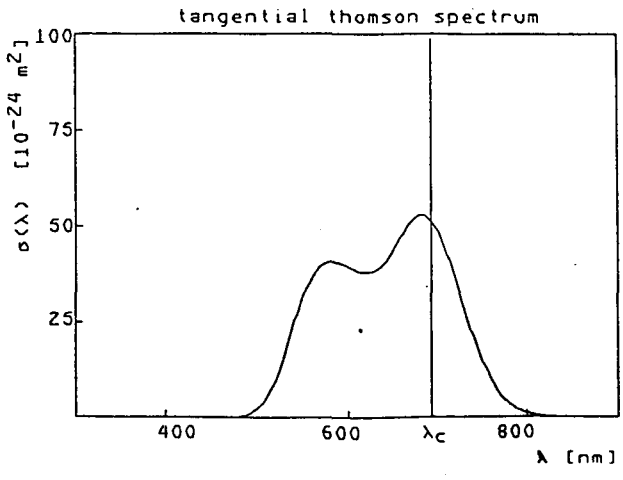

which confirms that, when $E < E_c$, runaways should be present only above the thermal velocity. In practical units the runaway field E_c can be written as :

$$E_c \simeq 4\left(\frac{n_e}{10^{19}}\right)\left(\frac{10^3}{T_e}\right)\left(\frac{\ln\Lambda}{15}\right) \qquad (V/m, m^{-3}, eV). \tag{3.36}$$

Although the runaway electrons are immune to Coulomb scattering, they still can interact with plasma waves. Resonant interaction between electrostatic waves and an electron travelling in the z direction takes place under the condition :

$$\omega - n\omega_{ce} - k_z v_z = 0. \tag{3.37}$$

The two most important resonances in our case are the Cherenkov resonance ($n = 0$) : $\omega = k_z v_z$, and the anomalous Doppler resonance ($n = 1$) : $\omega - \omega_{ce} - k_z v_z = 0$. These types of resonance can lead to instabilities of the electron-velocity distribution. One type of tail instability, described by Parail and Pogutse (1978), is a result of an interplay between the Cherenkov resonance and the anomalous Doppler effect and is developed if the highest velocity in the tail (v_b) exceeds some critical value. The combined action of the two instabilities will both cut off the runaway tail and form a plateau in the velocity distribution function. This happens for velocities :

$$v_b > 3(\omega_{ce}/\omega_{pe})^{3/2} v_c. \tag{3.38}$$

From the preceding it follows that the velocity distribution function for the electrons in a tokamak plasma that is subjected to an electric field, has a growing tail that is characterised by the critical velocities v_c and v_b. This is modelled by the bobtail distribution [Muschietti, 1982]. Because the applied field is directed along the toroidal magnetic field the electron distribution function for $v > v_c$ will be highly directional along the z axis. The above described features of the runaway distribution are mathematically denoted as :

$$f_{bobtail}(\beta) = \begin{cases} f_{eq}(\beta_\perp, \beta_\parallel), & \text{if } \beta < \beta_c; \\ f_{eq}(\beta_\perp, \beta_c), & \text{if } \beta_c \leq \beta \leq \beta_b; \\ f_{eq}(\beta_\perp, \beta_\parallel - \beta_b), & \text{if } \beta > \beta_b. \end{cases} \tag{3.39}$$

The example given below is based on an article of De Kluiver *et al.* (1987). In this article a typical TORTUR tokamak discharge is considered. Plasma parameters during the plateau stage of the discharge are : $n_e = 4{\cdot}10^{19} m^{-3}, T_e = 800eV, V_L = 6V, B_T = 2.9T$. The applied field follows from the loop voltage : $E \approx 2V/m$. With the help of the critical field ($E_c \approx 20V/m$), the critical velocity can be expressed in terms of the thermal velocity. Doing so, we get $v_c \approx 3.2 v_{the}$ (critical energy $\epsilon_c \approx 8keV$). The ratio of the electron cyclotron frequency ($\omega_{ce} \approx 5 \cdot 10^{11} rad/s$) to the electron plasma frequency ($\omega_{pe} \approx 4 \cdot 10^{11} rad/s$) determines the cut-off velocity of the runaway tail (v_b). According to equation (3.38) it follows $v_b \approx 3.9 v_c$. And we see that in this case the acceleration of the electrons from total runaway is limited, by beam-plasma interactions, up to $180keV$. The article under discussion mentions runaway energies up to $80keV$. Furthermore, experimental indications for the presence of a runaway electron population from electron cyclotron emission

Fig. 3.14e Calculated spectra for a bobtail distribution ($\beta_c = \beta_{the}$, see text in figures).

On this page the calculated spectra for the so-called "bobtail" distribution are show n. It is a prototype model for a run-away distribution.
The "bobtail" distribution is formed by a relativistic maxwellian, the body, on which a tail in tangential direction developes after some critical velocity, ßcrit, is exceeded. In the region between ßcrit and ßfin the distribution function takes the value of the maxwellian at ßcrit. In the case represented below the tail roughly contains 60% of the total amount of electrons.

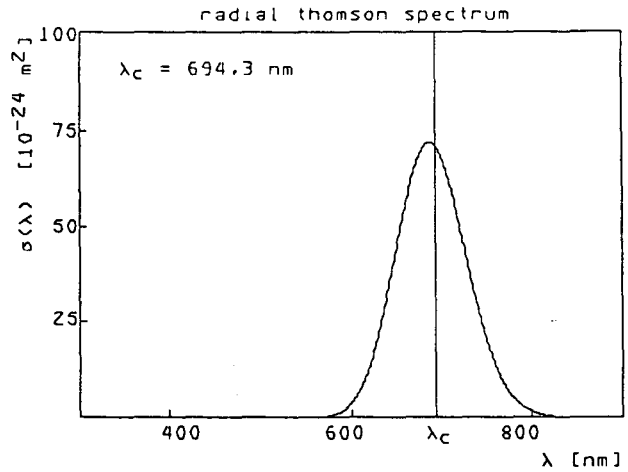

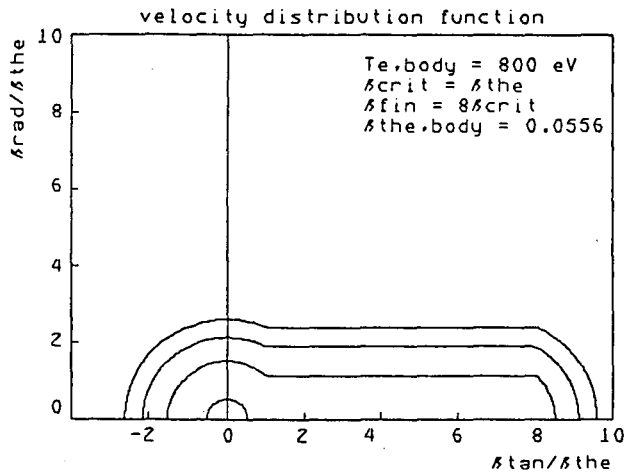

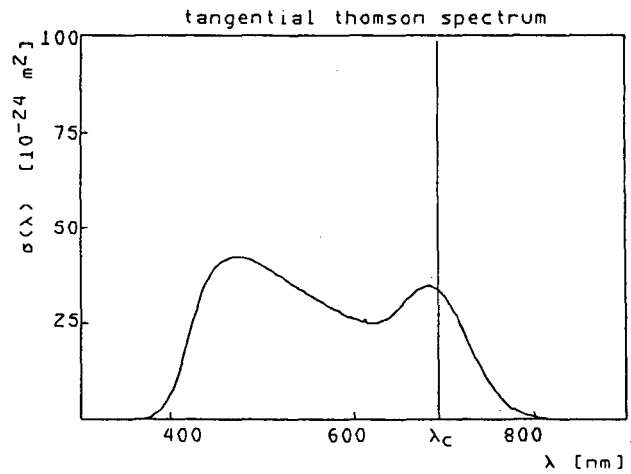

(ECE) spectroscopy and X-ray measurements are presented. Typical density numbers for the electron runaway population have been estimated and are in order of 0.01% of the electron density. In the bobtail model the relative electron tail density is determined by the choice of v_c and v_b. When the just obtained values for v_c and v_b are inserted in the bobtail distribution the corresponding relative electron tail density is about 0.015%, wich is concistent with the experimental findings.

By means of tangential-scattering, observation of the tangential tail distribution becomes possible. The observation of the runaway population in relation to the occurence of distortions on the Thomson-scattering spectra could hand a clue in clarifying this phenomenon. For this purpose a 4-channel polychromator was build (see *Fig.1.3*). This polychromator covers a spectral range from 305 to 595 nm. With this instrument tail temperatures up to about 20 keV can be surveyed. A tail distribution of several keV and with a partial density of $2 \cdot 10^{18} m^{-3}$ can be observed incidentally with an error of $\pm 20\%$.

From the preceding it becomes clear that in a normal discharge the partial runaway density at the center of the plasma is too small for recording. Looking at a low density discharge ($n_e = 2 \cdot 10^{19} m^{-3}, T_e = 800eV$), the critical velocity becomes $v_c \approx 2.3 v_{the}$ and the runaway electron density will be of order of the detection limit. In *Fig.3.14* the calculated spectra for bobtail distributions with $v_c = 2v_{the}$ and $v_c = v_{the}$ are shown. The values for v_b are chosen freely between 2 and 8. It should be stressed that the calculated spectra are merely intended to illustrate the features of scattering from non-thermal electron runaway distributions. Except for the case $v_c = v_{the}, v_b = 4v_c$ the chosen distribution functions are not realistic with respect to the TORTUR tokamak plasma. Nevertheless, the spectra for $v_c = v_{the}$ could be imagined to stem from Thomson-scattering measurements from an accelerator and the successive spectra for $v_c = 2v_{the}$ could be thought up depicting the growth of a runaway tail in a tokamak plasma.

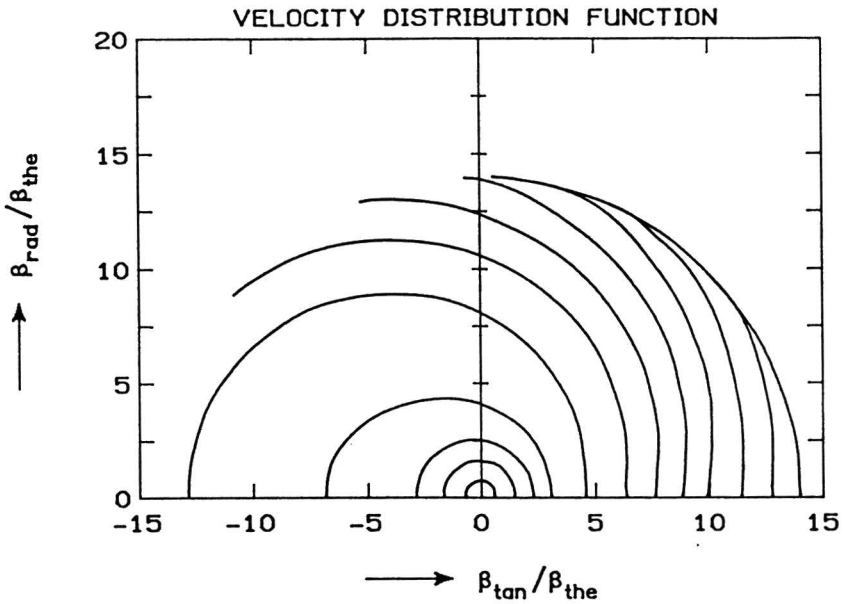

Fig.4.1 Electron velocity distribution function calculated from the Fokker-Planck code for typical TORTUR parameters ($T_e = 600eV, n_e(0) = 5 \cdot 10^{19}m^{-3}, Z_{eff} = 2, V_L = 5V$).

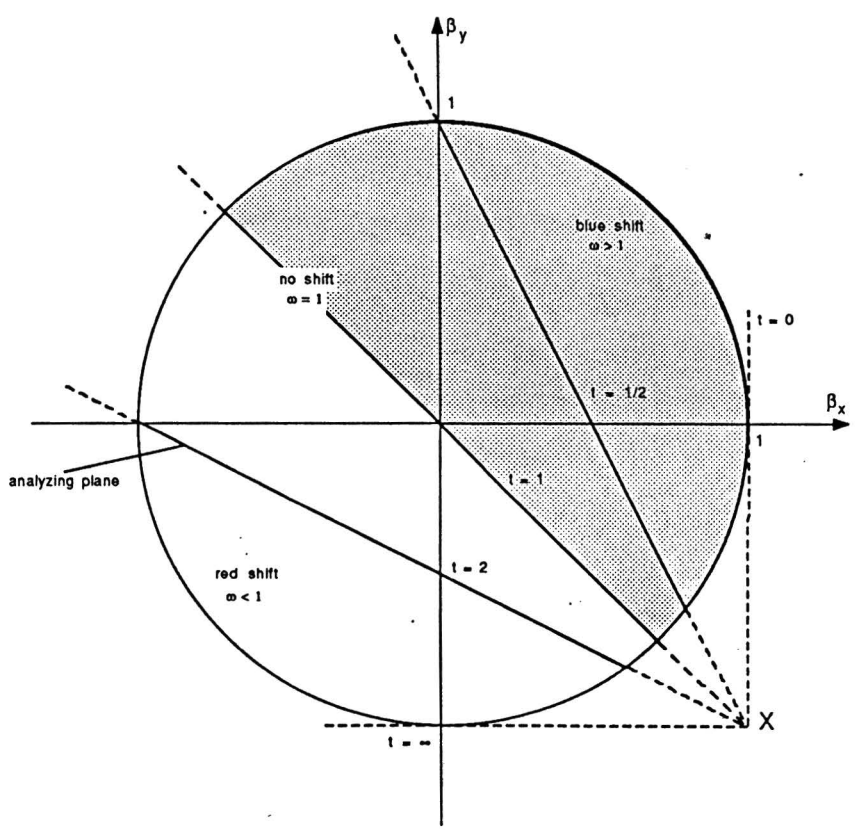

Fig.4.2 Construction of the analyzing planes for a 90° scattering experiment in the **radial** *direction. The laser beam is in the $-y$ direction and the scattered light is detected in the radial direction (x direction). All electrons with velocity vectors ending on any one plane contribute the same wavelength shift $\Delta\lambda$ at the detector. All planes pass through the axis which appears as the point X.*

IV. Geometrical considerations on Thomson scattering

In chapter III we already pointed out that according to relation (3.3) selection of a single frequency ω_s, with the help of a spectrometer, does not determine a single β but a whole group of velocities. The question "Which electrons are seen in the scattering experiment" is treated here in relation with a specific research item.

In the theory section of our institute a computercode is available that calculates the electron velocity distribution from the Fokker-Planck equation. The collision term in this equation is adapted to typical tokamak processes as the magnetic trapping of electrons (which results from the magnetic field configuration), the runaway process and of course Coulomb interactions. The involved plasma processes are slow compared to the Larmor frequency ω_c and vary slowly in space compared to the Larmor radius of the individual electrons. Such phenomena can be studied by the use of kinetic equations which average over the fast Larmor motion. These equations describe the evolution of the gyro-averaged distribution function :

$$\bar{f} = \frac{1}{2\pi} \int f \, d\phi, \tag{4.1}$$

where ϕ is the rapidly varying gyrophase. The averaged distribution $\bar{f}$ is a function of five phase variables $(x, y, z, \beta_{\parallel}, \beta_{\perp})$. In this case the solutions of the Fokker-Planck code are symmetric to the magnetic field. In the (β, θ, ϕ) coordinate system this means that $f(\beta)$ will be independent of ϕ. For this reason the distribution is calculated on a polar grid.

In *Fig.4.1* the electron velocity distribution function at $r = 0$ as derived from the code for specific TORTUR parameters ($Z_{eff} = 2, T_e = 600eV, n_e(0) = 5 \cdot 10^{19} m^{-3}, V_L = 5V$) is shown.

If we want to calculate the Thomson spectrum for radial or tangential scattering for the calculated velocity distributions we have to adjust the integral expression (3.8). For this we need a transformation between $(\beta_k, \beta_{k\perp}, \beta_{kT})$ and polar coordinates (β, θ, ϕ). Some parts in deriving the transformation matrix have already been made in this report. Consider the transformation between the following coordinate systems :

$$\begin{pmatrix} \beta \\ \theta \\ \phi \end{pmatrix} \longmapsto \begin{pmatrix} \beta_x \\ \beta_y \\ \beta_z \end{pmatrix} \longmapsto \begin{pmatrix} \beta_i \\ \beta_s \\ \beta_E \end{pmatrix} \longmapsto \begin{pmatrix} \beta_k \\ \beta_{k\perp} \\ \beta_{kT} \end{pmatrix}. \tag{4.2}$$

The relation between the cartesian coordinates $(\beta_x, \beta_y, \beta_z)$ and polar coordinates is the familiar one given by (3.15). The transformation between $(\beta_x, \beta_y, \beta_z)$ and $(\beta_i, \beta_s, \beta_E)$ was treated in section III.1.2 for a 90° scattering arrangement. Furthermore, the mapping between $(\beta_i, \beta_s, \beta_E)$ and the scattering coordinate system $(\beta_k, \beta_{k\perp}, \beta_{kT})$ is described by the inverse of matrix (3.6). The final result expresses $(\beta_k, \beta_{k\perp}, \beta_{kT})$ in polar coordinates (see Appendix IV.A1).

In addition we require the mapping of the volume $dV = d\beta_k \, d\beta_{k\perp} \, d\beta_{kT}$. The transformation of the volume is normally described by the *Jacobian* determinant :

$$dV = \left| \frac{\delta(\beta_k, \beta_{k\perp}, \beta_{kT})}{\delta(\beta, \theta, \phi)} \right| d\beta \, d\theta \, d\phi. \tag{4.3}$$

We will use another method to describe the transformation of the volume elements. This method will simplify the problem and will additionaly point out which electron velocities contribute to the intentensity scattered at the frequency ω_s. Our approach is firstly based on the isotropy of the calculated distribution function $f(\beta_\parallel, \beta_\perp)$ perpendicular to the magnetic field. Secondly, it is inspired by the property of the δ-function to select a plane in velocity space defined by constant β_k (see eq.(3.8); $\beta_k = (\omega - 1)/\sqrt{1+\omega^2}$ for 90° scattering). Let us look at the way this plane is positioned in the "laboratory" frame $(\beta_x, \beta_y, \beta_z)$. This is done the easiest by considering the argument of the delta function written in the form of equation (3.1). The electrons contributing to the spectrum at $\omega = \omega_s/\omega_i$ have to satisfy the constraint :

$$\omega = \frac{1-\beta_i}{1-\beta_s}. \tag{4.4}$$

Concentrating ourselfs for the moment on observations made in the horizontal plane ($\theta_s = 90°$) in radial direction ($\theta_o = 90°$) we can grasp the following picture. The incident wave propagates along the y axis ($\beta_i = -\beta_y$) and the scattered wave along the x axis ($\beta_s = \beta_x$). It follows from relation (4.4) :

$$\beta_x + t\beta_y + (t-1) = 0, \tag{4.5}$$

where $t = 1/\omega$. As sketched in *Fig.4.2*, for a given frequency, all electrons whose velocity vectors end in the indicated plane, defined by equation (4.4), contribute to the scattered power. We recall that successive points in the spectrum come from electron velocities lying in a series of parallel planes normal to the scattering vector $\mathbf{k}$. However, the scattering vector has not a fixed direction and planes of equal β_k will no longer be parallel in the velocity space $(\beta_x, \beta_y, \beta_z)$ corresponding to the experiment. This effect is taken into account by the terms in the transformation matrix between the coordinate system $(\beta_k, \beta_{k\perp}, \beta_{kT})$ and $(\beta_i, \beta_s, \beta_E)$ containing γ_s. Relation (3.10) shows the dependence of the direction of the scattering vector on the electrons' speed. For completeness we note that the following expression for γ_s is easily obtained :

$$\gamma_s = \arcsin \omega/\sqrt{\omega^2+1}, \tag{4.6}$$

where we have taken $\theta_s = 90°$. In interpreting the Thomson spectra we should be aware of the variable direction of the scattering vector. For most plasmas the variation of $\mathbf{k}$ with ω (cq. β_k) will be small. We can then assume that the spectrum observed at a constant angle θ_s corresponds to a spectrum for a fixed direction of $\mathbf{k}$. However, the dispersion of γ_s for scattering from $1keV$ electrons can be as large as 7°.

We now return to the original problem : the transformation of the volume elements. We recall that the velocity distribution is given (calculated) on a polar grid independent of the ϕ coordinate. Imagine the calculated points of the distribution in the horizontal plane ($\phi = 0$). Then we can, by use of symmetry of the distribution around the β_z axis, abstract the following picture for deriving the transformation of dV. [1] Consider a finit

[1] We have assumed that the magnetic field is in the z direction.

area dA in the horizontal plane. Because of the symmetry mentioned we may rotate this area around the β_z axis. Doing so, the points in dA will gradually intersect the oblique "interaction" planes. When in the horizontal plane a velocity vector is chosen with a β_x velocity component larger then the perpendicular distance from the origin to the planes of equal Doppler shift we have two intersections. In following this procedure we select all electrons in velocity space which contribute to the scattered power at the same frequency. The transformation of the area $dA = \beta\, d\beta\, d\theta$ can be visualised in the same manner. This is shown in *Fig.4.3* and treated in appendix IV.A2.

This concludes the mathematical treatment of the transformation of integral-expression (3.8) to (β, θ, ϕ) coordinates. At the moment, the code written for calculating the spectrum for a velocity distribution that is calculated on a two-dimensional polar grid (β, θ), being symmetric in the ϕ-component, shows severe numerical problems. These problems make it impossible to study the effects of small deviations from a Maxwellian distribution on the Thomson spectra. In case of the calculated electron-velocity distribution for typical TORTUR values the deformation of the distribution is essentially small. Looking at *Fig.4.1* we see that the electron-velocity distribution gets deformated from a Maxwellian for speeds larger than $\approx 2.5 v_{the}$. This means that the partial density of the electrons affected by the loop voltage ($V_L = 5V$) is in the order of 0.01%. These both values agree with the calculations made earlier (section III.3) using a simple runaway distribution.

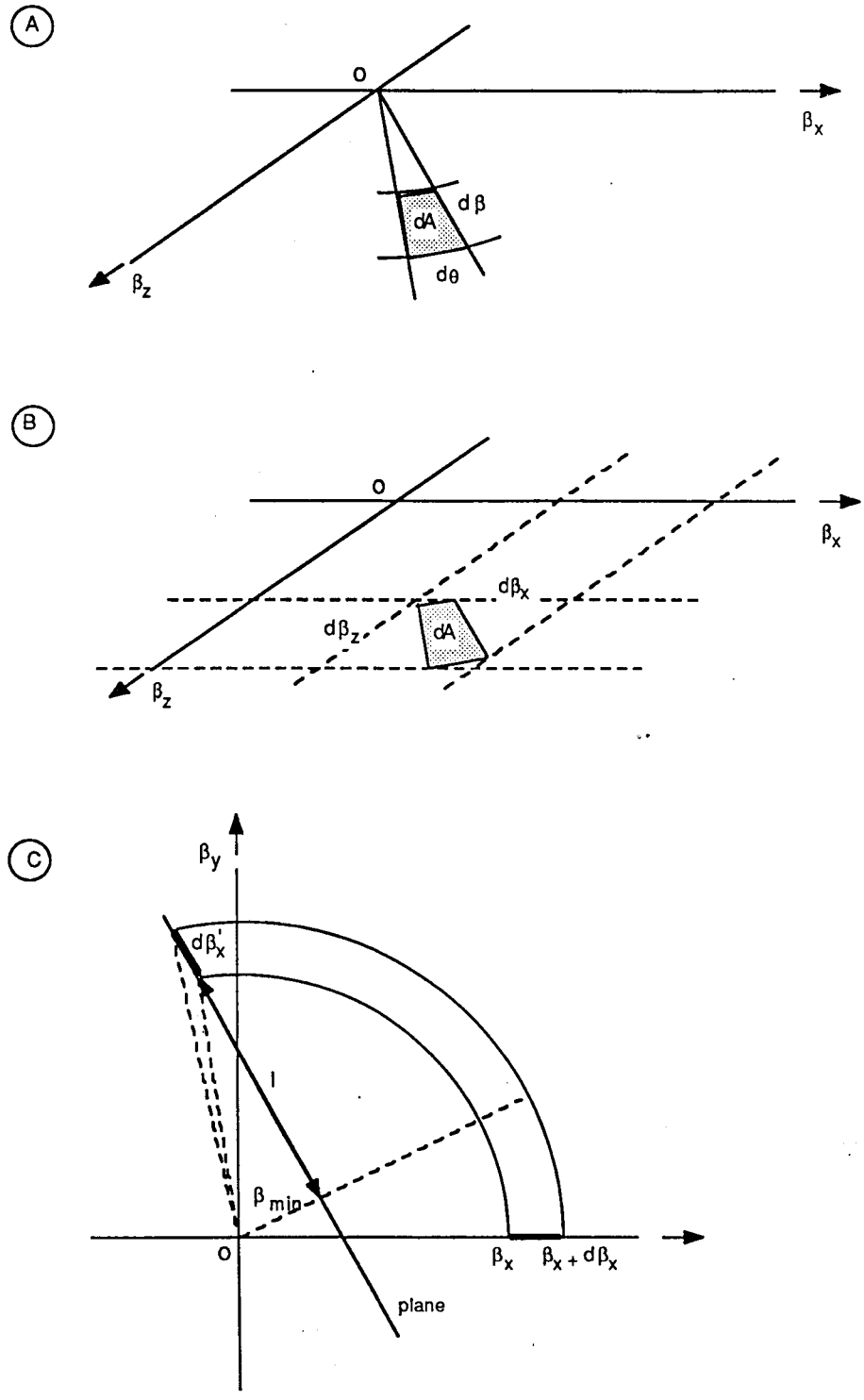

Fig.A2.1 Transformation of the area dA for radial scattering :
A) finit area dA in the horizontal plane;
B) definition of $d\beta_x$ and $d\beta_z$;
C) transformation of the β_x component.

IV.A1 Transformation matrix from $(\beta_x, \beta_y, \beta_z)$ *to* $(\beta_k, \beta_{k\perp}, \beta_{kT})$

We want to express the scattering coordinates $(\beta_k, \beta_{k\perp}, \beta_{kT})$ in terms of the coordinates $(\beta_x, \beta_y, \beta_z)$. This transformation is done in two steps. In the first step the $(\beta_x, \beta_y, \beta_z)$ frame is transformed to the $(\beta_i, \beta_s, \beta_E)$ system. For observations made in the horizontal plane at the angle θ_o we can write, according to (3.21) :

$$\begin{pmatrix} 0 & -1 & 0 \\ \sin\theta_o & 0 & \cos\theta_o \\ -\cos\theta_o & 0 & \sin\theta_o \end{pmatrix} \begin{pmatrix} \beta_x \\ \beta_y \\ \beta_z \end{pmatrix} = \begin{pmatrix} \beta_i \\ \beta_s \\ \beta_E \end{pmatrix}. \qquad (4.A1.1)$$

The transformation between the $(\beta_i, \beta_s, \beta_E)$ and $(\beta_k, \beta_{k\perp}, \beta_{kT})$ frames is given by the inverse matrix (3.6) :

$$\begin{pmatrix} -\cos\gamma_s & -\cos(\gamma_s+\theta_s) & 0 \\ \sin\gamma_s & \sin(\gamma_s+\theta_s) & 0 \\ 0 & 0 & -1 \end{pmatrix} \begin{pmatrix} \beta_i \\ \beta_s \\ \beta_E \end{pmatrix} = \begin{pmatrix} \beta_k \\ \beta_{k\perp} \\ \beta_{kT} \end{pmatrix}. \qquad (4.A1.2)$$

Connecting (4.A1.1) and (4.A1.2) we get :

$$\begin{pmatrix} -\sin\theta_o\cos(\gamma_s+\theta_s) & \cos\gamma_s & -\cos\theta_o\cos(\gamma_s+\theta_s) \\ -\sin\theta_o\sin(\gamma_s+\theta_s) & -\sin\gamma_s & \cos\theta_o\sin(\gamma_s+\theta_s) \\ \cos\theta_o & 0 & -\sin\theta_o \end{pmatrix} \begin{pmatrix} \beta_x \\ \beta_y \\ \beta_z \end{pmatrix} = \begin{pmatrix} \beta_k \\ \beta_{k\perp} \\ \beta_{kT} \end{pmatrix}, \qquad (4.A1.3)$$

where $\theta_s = 90°$. For light scattering from non-relativistic electrons ($\gamma_s \approx \pi/4$) in radial direction ($\theta_o = \pi/2$) equation (4.A1.3) is simplified by :

$$\frac{1}{\sqrt{2}} \begin{pmatrix} 1 & 1 & 0 \\ 1 & -1 & 0 \\ 0 & 0 & -\sqrt{2} \end{pmatrix} \begin{pmatrix} \beta_x \\ \beta_y \\ \beta_z \end{pmatrix} = \begin{pmatrix} \beta_k \\ \beta_{k\perp} \\ \beta_{kT} \end{pmatrix}. \qquad (4.A1.4)$$

IV.A2 Transformation of the area dA

Consider a finit area dA defined in the horizontal plane in a polar grid (see *Fig.A2.1a*) :

$$dA = \beta\, d\beta\, d\theta, \qquad (4.A2.1)$$

and a plane descibed by :

$$\beta_x + t\beta_y + (t-1) = 0. \qquad (4.A2.2)$$

The smallest distance from the origin to this plane, r_{min}, is given by :

$$r_{min}^2 = \frac{(1-t)^2}{1+t^2}. \qquad (4.A2.3)$$

When the area dA is rotated around the β_z axis a ring is formed. This cylindrical shell will intersect the plane if dA was positioned in the region where $\beta_x > r_{min}$. Let us look at the area dA' of the intersection. We first note that a rotation around the β_z axis will leave the form of the area in the β_z direction unchanged. So, we only have to consider the deformation of β_x component of dA. When the β_x component $d\beta_x$ of dA is stretched out to the length $d\beta'_x$, we may write :

$$dA' = dA\frac{d\beta'_x}{d\beta_x}. \tag{4.A2.4}$$

From *Fig.A2.1c* we can derive :

$$l^2 = \beta_x^2 - r_{min}^2$$

$$(l + d\beta_x)^2 = (\beta_x + d\beta_x)^2 - r_{min}^2, \tag{4.A2.5}$$

and thus :

$$d\beta'_x = \sqrt{(\beta_x + d\beta_x)^2 - r_{min}^2} - \sqrt{\beta_x^2 - r_{min}^2}, \tag{4.A2.6}$$

with $\beta_x = \beta \sin\theta$ and $d\beta_x = |\sin\theta|\, d\beta + |\beta \cos\theta|\, d\theta$.

For tangential scattering a similar method can be followed in obtaining the transformation of an area dA in the horizontal plane. In this case formula (4.A2.6) is altered by substitution of r_{min} by r^*_{min} :

$$r^*_{min}{}^2 = \sqrt{2} r_{min}^2 - z^2, \tag{4.A2.7}$$

where $\beta_z = \beta \cos\theta$. Additionally, the β_z component will be transformed by approximately a factor $\sqrt{2}$.

Summary

• "Isotropic" code

A code is written for calculating the Thomson spectrum for an isotropic electron-velocity distribution function, which is tested by means of an analytical expression for the Thomson spectrum for a relativistic Maxwellian.

• "Anisotropic" code

A code is written for calculating the Thomson spectrum for an anisotropic electron-velocity distribution function, which is tested by means of calculated spectra from the "isotropic" code and simple model distribution functions (e.g. "electron-beam").

• Detection of tail populations

Calculations using a simple runaway distribution as well as the calculated electron-velocity distribution from the Fokker-Planck code show that at a normal discharge the partial runaway density ($\approx 0.01\%$) at the center of the plasma is to small to be detected by the 4-channel polychromator.

• Detection of non-thermal distortions

Local perturbations with a partial density of 1% in velocity space can be detected by the 20-channel polychromator.

• Interpretation of Thomson spectra

For a given frequency, any electron velocity in the "analysing" plane will contribute at a different rate to the scattered power. The position of the "analysing" plane in velocity space is determined by the Doppler shift and the scattering geometry.

• Suggestions

⋆ A mathematical treatment is given for a code that calculates the spectrum for a distribution which is calculated on a polar grid. Such a code would offer the possibility of calculating the Thomson spectrum for any calculated velocity-distribution from the Fokker-Planck code.

⋆ After the statistical analysis of the radial and tangential Thomson spectra measured at the TORTUR tokamak the "anisotropic" code is to be used for finding a set of electron-velocity distributions corresponding to the data. This will hopefully give further indication about the physical process(es) involded in the occurence of the non-thermal features on the Thomson spectra at TORTUR.

⋆ Be hard on yourself and mild to another.

References

Barth C.J., "A High Transmission, 20-Channel Polychromator for the Thomson-Scattering Diagnostic of TORTUR III", Rijnhuizen Report 84-156 (1984).

Barth C.J., "Tangential Thomson Scattering", Rijnhuizen Report 87-173 (1987).

Bartiromo R., Buratti P., Pieroni L. and Tudisco O., "Non-Thermal Electron Distribution Function in the FT Tokamak", in *Proceedings, Ninth European Conference*, Oxford (1979), 47.

Blokh M.A. and Larionova N.F., "Non-Maxwellian Velocity Distribution Functions Detected in the L-2 Stellarator by Laser Scattering", Sov. J. Plasma Phys. **7**, 31 (1981).

De Kluiver H., Barth C.J. and Donné A.J.H., "Current Driven Turbulence and Microturbulent Spectra in the TORTUR Tokamak", Plasma Phys. Controlled Fusion **30**, 699 (1988).

Evans D.E. and Katzenstein J., "Laser Light Scattering in Laboratory Plasmas", Rep. Prog. Phys. **32**, 207 (1969).

Knoepfel H. and Spong D.A., "Review Paper : Runaways in Toroidal Discharges", Nucl. Fusion **19**, 785 (1979).

Kukushkin A.B., "Incoherent Scattering of Light by a Finite Volume of Relativistic Plasma", Sov. J. Plasma Phys. **7**, 63 (1981).

Matoba T., Itagaki T., Yamauchi T. and Funahashi A., "Analytical Approximations in the Theory of Relativistic Thomson Scattering for High Temperature Fusion Plasma", Jap. J. Appl. Phys. **18**, 1127 (1979).

Mattioli M., "Incoherent Light Scattering from High Temperature Plasmas", EUR-CEA-FC-752 (1974).

Muschietti L., "Interaction Ondes-Particules : Electrons ≪Runaway≫ et Ondes HF dans un Plasma Magnetise", thesis at Lausanne nr. 455 (1982).

Nielsen P., "Thomson Scattering in High Temperature Devices", in *Proceedings, Course on Diagnostics for Fusion Reactor Conditions*, Varenna Vol.I (1982), 225.

Parail V.V. and Pogutse O.P., "The Kinetic Theory of Runaway Electron Beam Instability in a Tokamak",

Nucl. Fusion **18**, 303 (1978).

Pieroni L. and Segre S.E., "Observation of Non-Maxwellian Electron Distribution Functions in the Alcator Device by Means of Thomson Scattering and Their Interpretation",
Phys. Rev. Lett. **34**, 928 (1975).

Salzmann H., "Thomson Scattering",
in *Proceedings, Workshop on Basic and Advanced Diagnostic Techniques for Fusion Plasmas*,
Varenna, Vol.II (1986), 477.

Tartari U., "Thomson-Scattering Measurements and Non-Thermal Regimes in the Thor Plasma",
FP-84/20 (1984).

Williamson J.H., Clarke M.E., "Construction of Electron Distribution Functions from Laser Scattering Spectra",
J. Plasma Phys. **6**, 211 (1971).

Zhuravlev V.A. and Petrov G.D., "Scattering of Light by Electrons of a High Temperature Plasma",
Opt. Spectrosc., **33**, 19 (1972).